1290

UNIVERSIDADE Ð COIMBRA

Gonçalo José da Silva Rodrigues

AUTONOMOUS TARGETING SYSTEM FOR A FIREFIGHTING DRONE –
DETECTION AND LOCALIZATION OF HOTSPOT

Dissertação no âmbito do Mestrado em Produção e Projeto orientada pelo/a Professor/a Doutor/a Carlos Xavier Pais Viegas e apresentada ao Departamento de Engenharia Mecânica da Faculdade de Ciências e Tecnologia da Universidade de Coimbra.

Outubro de 2021

F A C U L D A D E D E
CIÊNCIAS E TECNOLOGIA
UNIVERSIDADE Ð
COIMBRA

1 2 9 0

Autonomous Targeting System for a Firefighting Drone

Submitted in Partial Fulfilment of the Requirements for the Degree of Master in Mechanical Engineering in the speciality of Production and Project.

Sistema De Mira Autónomo Para Um Drone De Combate A Incêndios

Author
Gonçalo José da Silva Rodrigues

Advisor[s]
Carlos Xavier Pais Viegas
Babak Chehreh

Jury

President	**Professor Doutor Miguel Rosa Oliveira Panão** **Professor Auxiliar da Universidade de Coimbra**
Vowel[s]	Professor Doutor **Carlos Xavier Pais Viegas** Professor Convidado da Universidade de Coimbra
	Professor Doutor **Jorge Rafael Nogueira Raposo** Professor Convidado da Universidade de Coimbra
	Professor Doutor **Pedro Mariano Simões Neto** Professor Auxiliar da Universidade de Coimbra
Advisor	Professor Doutor **Carlos Xavier Pais Viegas** Professor Convidado da Universidade de Coimbra

Coimbra, October 2021

To my parents, Marta e Paulo.

To my girlfriend, Carolina.

To my family.

To my best friends, from Chouto and Coimbra.

ACKNOWLEDGEMENTS

The greatest gratitude to the following people, who in different ways supported me over the years and contributed to my personal and academic evolution. A sincere thank you to everyone!

To the advisor, Prof. Dr. Carlos Xavier Pais Viegas.

For all the availability given throughout this project, in any circumstance.

To the co-supervisor, Eng. Babak Chehreh.

For all his help throughout this thesis.

To José Pedro Correia.

For all his help throughout this thesis, which was essential.

To my parents, Marta e Paulo.

For being the people who support me in everything in my life, for working hard so that I never lack for anything, and for giving me the opportunity to take a university degree.

To my girlfriend, Carolina.

For always being available to support me, and for always motivating me to give my best.

To my friends João Oliveira, Bruno Mourato and Paulo Custódio.

For the pleasure of having grown up with them, for the friendship, for the humility they transmit and for knowing that I can always count on them.

To my friends from Coimbra, Ruben Nascimento, Rafael Jorge, Rui Coimbra and Pedro Costa.

For friendship, for sharing very good moments, for the mutual support that we gave each other to face this university trip, and for the excellent values that they transmit.

Abstract

Forest fires are a very present reality in the Portuguese panorama, possibly being the natural disaster that most affects the country, both in environmental terms, as well as in economic and social terms. Firefighting is a very dangerous type of activity that sometimes takes the life of those who combat it. To reduce the risk to which firefighters are subject, it is necessary to develop new strategies and techniques that preserve the physical integrity of firefighter. For this, it makes sense to resort to technological advances already made to try to develop a solution that helps firefighters fight fires without constantly being in danger.

This work consists of the development of an autonomous targeting system that must detect and locate hotspots through an IR sensor, and that will be incorporated in a drone that must work as autonomously as possible. The main objectives of this work are the development of an algorithm that determines the location of the hotspot, the study of the wind effect on the waterjet that will hit the hotspot, and the development of an algorithm that determines the correct movements so that the waterjet hits accurately on the hotspot.

For the development of this work, the IR sensor Flir Lepton 3.5 was used, whose objective is to generate a matrix of values that indicate the temperature in each pixel. It will be this sensor that will indicate the position in which the hotspot is located. Another key sensor is the PX4Flow. This sensor has a sonar attached that allows the user to know accurately how high the drone is from the ground. This sensor is very important in defining the trajectory of the waterjet. There is also a flight controller, which is the Pixhawk 4 mini, and which is responsible for indicating parameters such as the "yaw" angle at which the drone is. All information is sent to the Adafruit Huzzah32 microcontroller. This device is responsible for communication via Wi-Fi between the drone and the user.

The first steps of this work consisted of determining the distance at which the hotspot was from the drone, according to the characteristics of the matrix generated by the IR sensor. Then the trajectory of the waterjet was determined. For this, it was necessary to analyze the effect of airflow on a waterjet in a wind tunnel to determine its aerodynamic characteristics. Knowing the distance at which the hotspot is from the drone and knowing the trajectory of the waterjet, it is possible to know the movement that the drone must do to be aligned with the hotspot. The next step of this work consisted of making the communication between the sensors and controllers. For this, communication protocols, like I^{2}C and SPI, were used. A C# interface was also developed that allows the user to remotely control the drone and, at

the same time, receive data via Wi-Fi in real-time for all the required parameters. The last step of this work consisted of conducting experimental tests on this entire system installed in the drone, to verify if the entire theoretical approach was done correctly.

Keywords Fire, Forest, Firefighting, Drone, Hotspot, IR Sensor, Remote Control.

Resumo

Os incêndios florestais são uma realidade bem presente no panorama português, sendo possivelmente a catástrofe natural que mais afeta o país, quer em termos ambientais, como económicos e sociais. O combate aos incêndios constitui um tipo de atividade muito perigosa, e que por vezes tira a vida a quem a realiza. Na tentativa de reduzir o risco a que os bombeiros estão sujeitos, é necessário desenvolver novas estratégias e técnicas que permitam preservar a integridade física dos bombeiros. Para isso faz sentido recorrer aos avanços tecnológicos já feitos para tentar desenvolver uma solução que auxilie os bombeiros no combate aos incêndios sem que estes estejam constantemente sob perigo.

Este trabalho consiste no desenvolvimento de um sistema de mira automática que deve detetar e localizar pontos quentes através de um sensor IR, e que será incorporado num drone que deve funcionar da forma mais autónoma possível. Os principais objetivos deste trabalho são o desenvolvimento de um algoritmo que determine a localização do ponto quente, o estudo do efeito do vento no jato de água que irá atingir o ponto quente, e o desenvolvimento de um algoritmo que determine o ângulo "yaw" do drone e o ângulo "tilt" da agulheta de forma que o jato de água incida sobre o ponto quente.

Para o desenvolvimento deste trabalho foi utilizado o sensor IR Flir Lepton 3.5, cujo objetivo é gerar uma matriz de valores que indiquem a temperatura em cada pixel. Será este sensor que indicará qual a posição em que se encontra o ponto quente. Outro sensor fundamental é o PX4Flow. Este sensor tem acoplado a si um sonar que permite ao utilizador saber de forma muito aproximada a que altura se encontra o drone do solo. Este sensor é muito importante na definição da trajetória do jato de água. Existe ainda um controlador de voo, que é o Pixhawk 4 mini e que é responsável por indicar parâmetros tais como o ângulo "yaw" a que o drone se encontra. Toda a informação é enviada para o microcontrolador Adafruit Huzzah32. Este dispositivo é responsável pela comunicação via Wi-Fi entre o drone e o utilizador.

As primeiras etapas deste trabalho consistiram em determinar a distância a que o ponto quente se encontrava do drone, de acordo com as características da matriz gerada pelo sensor IR. De seguida foi determinada a trajetória do jato de água. Para isso foi necessário analisar o efeito de um escoamento de ar sobre um jato de água num túnel de vento de forma

a determinar as suas características aerodinâmicas. Sabendo a distância a que o ponto quente está do drone e sabendo a trajetória do jato de água, é possível saber qual o movimento que o drone tem de realizar para se enquadrar com o ponto quente. A etapa seguinte deste trabalho consistiu em fazer a comunicação entre os sensores e os controladores. Foi ainda desenvolvida uma interface em C# que permite ao utilizador controlar remotamente o drone e, ao mesmo tempo, receber dados via Wi-Fi em tempo real de todos os parâmetros requeridos. A última etapa deste trabalho consistiu em realizar ensaios experimentais a todo este sistema instalado no drone, de forma a verificar se toda a abordagem teórica foi feita de forma correta.

Palavras-chave: Incêndio, Floresta, Combate a Incêndios, Drone, Ponto Quente, Sensor IR Controlo Remoto.

Contents

LIST OF FIGURES

LIST OF TABLES

1. INTRODUCTION

Portugal is one of the most affected countries by forest fires in Europe. To this contributes its location in the globe, its characteristic climate, and global warming. Every year, these fires cause environmental, social, and economical problems. According to Global Wildfire Information System (GWIS), from 2002 to 2019, Portugal is the second country in Europe whose ratio between burned area and country size is higher, only surpassed by Ukraine. The data that shows this is represented in Figure 1, and it was taken from [1]
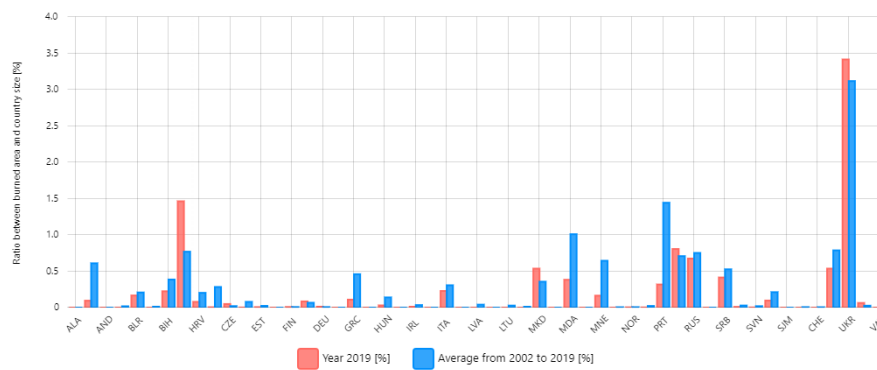
Figure 1 - 2019 Burned Area vs Historical Average Burned Area [2002-2019] (extracted from[1])

Bearing in mind that is impossible to extinct this catastrophe, is very important to be able to minimize it. To do this, it is necessary to use not only existing fire prevention and firefighting techniques but also to use science and engineering to develop new techniques and new instruments that are effective in fighting the fire.

The use of unmanned aerial vehicles (UAV) can be an alternative technique for firefighting. This thesis work introduces a new methodology for UAVs to autonomously detect and localize hotspots and accurately direct a waterjet to these hotspots, taking into account the wind disturbance on the waterjet trajectory. The UAV has to couple a set of gadgets like a thermal camera and an altitude sensor. To accurately calculate the waterjet trajectory is fundamental to consider the wind velocity and direction.

The SAP - Sistema Agulheta Auto Portante prototype is financed by Portugal 2020 - Centro 2020 - European Fund for Regional Development (Operational Program of the Center) and the research work was partially funded by the Project F3 Desenvolvimento de

1.1. Motivation

Nowadays there are many ways to fight fires, including the use of airplanes and helicopters. The use of airplanes is a very efficient way of combat, as they allow the transport of a large amount of water to areas that are difficult to reach. The aircraft flies at high speed (approximately 160 km/s) just above the surface of a lake reservoir scooping up copious amounts of water into header tanks. In just 12 seconds, the plane can scoop up to 6000 litters of water, to be subsequently dropped onto nearby fires raging out of control. Another advantage is that there are airplanes that can immerse themselves in lakes to refill, without the need for the help of others to supply them. A good example of this type of airplane is the Canadair CL-415 [2]. This airplane was developed in the mid-'90s and allows for carrying approximately 3 tons of water. Figure 2 shows an example of this plane.

Figure 2 - Example of a Canadair CL-415 (extracted from [2])

Another way to fight fires by air is through helicopters. Helicopters are very agile combat vehicles, but with the inconvenience of being very limited in terms of the capacity to store water. In this way, they are more suitable for small fires.

Despite being an efficient technique, the use of manned aerial vehicles to fight fires can be very dangerous, especially in large fires. In many cases, these flights are made with very little visibility, which can lead to aircraft crashing with electric cables or with hills and trees, when the terrain is uneven. This type of accident often leads to the death of aircraft crew. In Portugal, the number of rural fires has been decreasing since 2010 as Figure 3 shows. However, this figure also shows that the number of aircrafts accidents was superior in the second half of 10's decade, comparing with first half. These data were taken from GPIAAF (Gabinete de Prevenção e Investigação de Acidentes com Aeronaves e Acidentes Ferroviários) [3] and PORDATA [4].
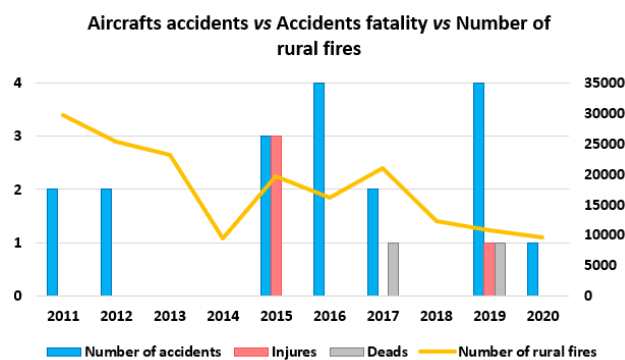
Figure 3 - Number of aircrafts accidents and their fatality (extracted from [3] and [4])

To reduce the number of fatalities in firefighting teams, new technologies should be sought, including robots and autonomous systems. This prevents a greater number of firefighters from being exposed to possible dangers like severe burns, intoxication, and injuries from falling trees. An example of a robot designed to fight fires is the Colossus robot [5], developed by Shark-robotics. This robot is handled by remote control, being able to be controlled up to 500m away. Besides, it is equipped with a thermal camera and also sensors that detect gases resulting from combustion. Figure 4 shows this robot fighting the fire that occurred in the Notre-Dame cathedral in France.

Figure 4 - Colossus fighting fire in Notre-Dame (extracted from [5]**)**

It makes sense to continue to develop new and better device prototypes that help firefighters fight fires in the safest possible way. The development of this thesis consists of creating a prototype of an unmanned aircraft (UAV) to continue using these new firefighting techniques. There will also be an effort to make this aircraft as autonomous as possible.

1.2. Objectives

The general goal of this thesis is to develop a prototype of an unmanned aircraft (UAV) for fighting fires with autonomous operation. For this, a drone with a directional nozzle will be used. This system must be able to:

- Obtain the surrounding wind speed and direction based on the drone's internal sensors (IMU);
- Detect a fire spot (hotspot) using an onboard IR sensor;
- Determine the relative location between the fire spot (hotspot) and the drone, by combining the data from the onboard IR sensor and the drone's optical flow sensors;
- Determine the required drone movement for targeting the hotspot, through an algorithm that considers the relative distance between the drone and the fire spot, and the external wind disturbance on the waterjet;
- Autonomously actuate the nozzle tilt angle and the drone's yaw angle.

The mentioned goals were distributed by two thesis works, and for this specific thesis, the outlined objectives were:

- Detect hotspots using an IR sensor onboard the UAV;

- Develop an algorithm to determine the location of the hotspot, relative to UAV;

- Study the effect of the wind on the waterjet that will reach the hotspot;

- Develop an algorithm to determine the required UAV movements for accurately targeting the hotspot location.

1.3. Methodology

In this chapter, an approach will be made to the components used to correctly locate the hotspot. It will also be described how all these components will interconnect to achieve the objectives defined successfully. Figure 5 shows the assembly of some of the components that will be covered in this chapter, like Optical Flow, Lepton 3.5, water targeting system, and vision sensor.
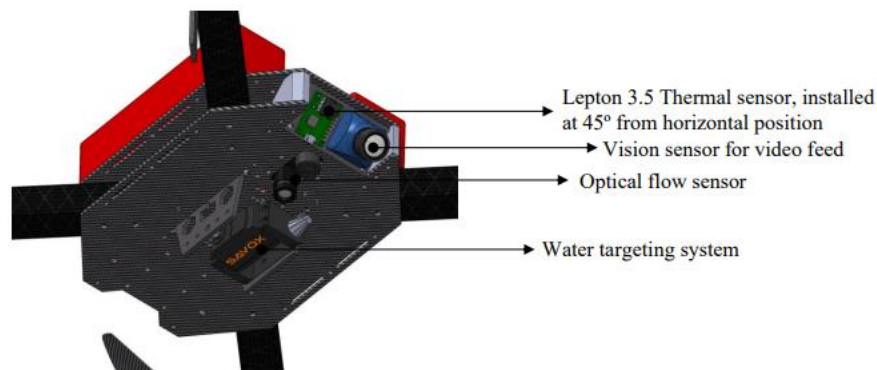
Figure 5 - Component representation

The PX4Flow optical flow sensor is responsible for measuring the distance to the ground of the UAV with great precision, using a combination of sonar and vision sensors. This sensor must be installed in such a way that the direction of the measurement performed is perpendicular to the base of the UAV. This ensures a correct distance measurement. Lepton 3.5 is the main component of the hotspot detection system and works through infrared radiation. Its measurement features are the high thermal sensitivity and image resolution, for its size and cost.

The detection system is connected firstly to Raspberry Pi 4. After that, Raspberry Pi 4 is connected to the Adafruit Huzzah32 microcontroller. The purpose of Raspberry Pi 4 is the reading of Lepton 3.5 sensor. In this way, it is possible to combine the output given by the infrared sensor with the output given by the Optical flow sensor. The purpose of this combination is to calculate the rotation that the drone has to do for the waterjet reaches the hotspot. The calculation of the movement of the drone is done considering the action of the wind on the waterjet. For this, it is necessary to measure the wind speed and direction and export the data collected to the microcontroller. This entire description is outlined in the selected area in Figure 6.
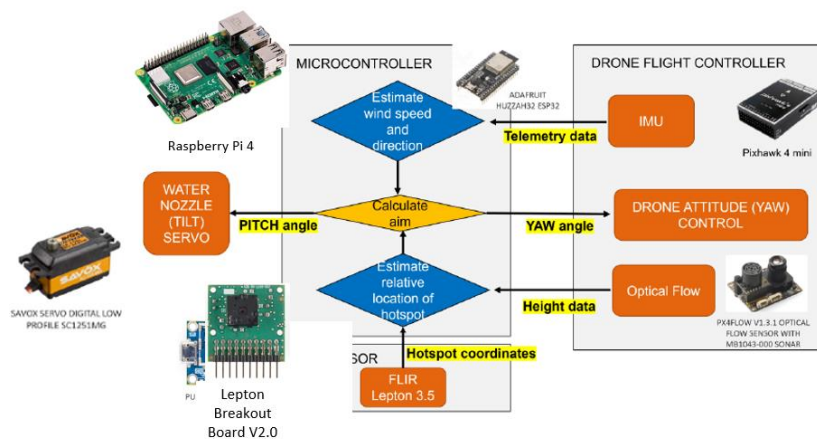
Figure 6 - Schematic of the interaction of UAV components

Figure 7 shows a 3D model of the drone used. This drone weighs about 3.2 kg and has a flight autonomy of approximately 10 minutes. To have an ideal weight distribution, the drone allows the assembly of the batteries to be done on its bottom or top. Another very important feature is the vibration damping that occurs in all sensory systems and IMU. This is advantageous since the error of the measurements made is mitigated and these systems are also protected from any damage caused by high frequency vibrations.

Figure 7 – 3D model of the drone

1.4. Outline

This dissertation is organized as follows:

Introduction: in this chapter, an introduction to the theme of this thesis is done and the existing problem is exposed. Several strategies for technology-based firefighting and a description of some components of the drone and their architecture are also preserved.

State of the art: Research works and articles related to the topic of the thesis and an evaluation and comparison of different research strategies are preserved.

Work development: This chapter is divided into some subchapters: one subchapter relates the detection and location of the hotspot and analyses the matrix read by the Lepton 3.5 sensor. The next one is responsible for analysing the wind effects on the waterjet. The thirst subchapter consists of the determination of the targeting algorithm, and the movement that the UAV has to do. The last one discusses the work carried out with the sensors, such as their calibration and implementation in the UAV, and the GUI implementation.

Experimental tests and results: The results and experimental tests are used to validate and complement the theoretical approach proposed. This chapter describes the experimental tests methodology and the results.

Conclusion: This chapter is used to relate if the main objectives were completed and to take some remarks about all this work. It is also important to discuss in this chapter the results obtained in experimental tests, and the improvements that can be made in the future.

2. STATE OF THE ART

2.1. Firefighting drones

In [6] patented a firefighting system consisting of an unmanned and remotely controlled aerial vehicle, which is connected to a water supply tank through a hose. This system allows not only the projection of water directly into the fire but also the projection of liquid retardant that attenuates the progress of the fire.

The main virtues of this system are the easy adaptation to any vehicle with a water tank and also the implementation of a temperature sensor. This sensor allows a continuous search for hotspots. Also, the fact that it has few components makes the drone lighter, reducing energy costs to keep it running.
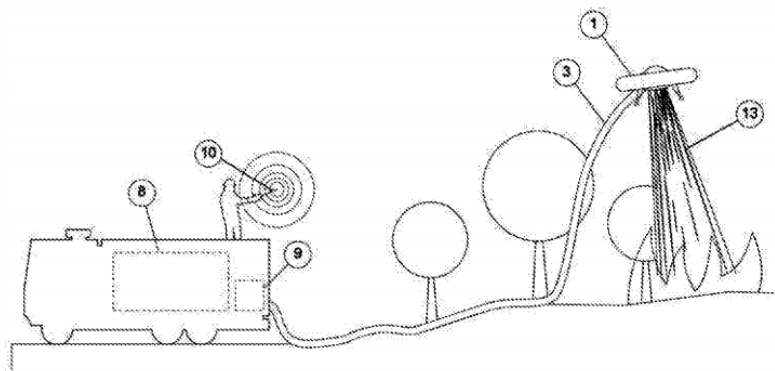
Figure 8 - Ilustration of how the drone is used (extracted from [6])

Through Figure 8, it is possible to see, in general, how this drone is used. The figure shows not only the drone in action but also the user to operate it remotely, close to the supply tank.

The second reference shown is a French patent [7] published in 2020. This patent presents a firefighting system very similar to the system that will be treated in this thesis. The drone is connected to a water supply tank through a hose, which allows water to be brought to the nozzle of the drone. This nozzle is responsible for pointing the waterjet at the hotspot.

The main advantages are the high ease of maneuvering the drone and also the fact that it is controlled via Wireless. The presence of a camera is also important to monitor from a distance what is happening from the perspective of the drone. The biggest disadvantages

are the lack of a thermal camera, making it impossible to detect hotspots, and also the disregard given to the effects of the wind on the waterjet. This aspect can be decisive for the success of the operation since the waterjet may not targeted to the appropriate location.

The most recent reference in this review of the state of the art regarding firefighting drones is [8]. This firefighting system includes the use of a supply tank, similar to what happens in other references, and a waterjet system that focuses on the hotspot. This system is characterized by the existence of three drones, as shown in Figure 9. According to this figure, drone 135 serves only for reconnaissance. This reconnaissance is done through a thermal camera that detects the hotspots. This reconnaissance drone is used at higher altitudes than direct firefighting drones and has independent movement. Besides, it is capable of transmitting information to a controller via Wireless. Regarding direct fire drones, these are divided into an auxiliary drone (132) and a combat drone (131), which are coupled through a hose. The auxiliary drone, in addition to being able to project the waterjet into the hotspot, can simultaneously route water from the supply tank to the combat drone (131). The combat drone (131) has the sole function of projecting the waterjet over the fire.
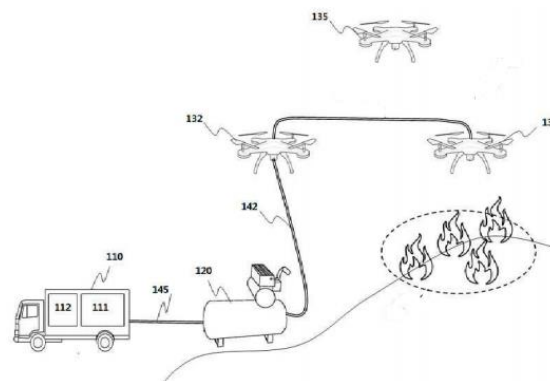
Figure 9 - Representation of the 3 drones used in this system (extracted from [8])

The main advantage of this system is the existence of more than one drone for direct firefighting. This can lead to the achievement of objectives in a faster and more effective way. Another advantage is the possibility of coupling direct combat drones to more than one nozzle. The weakness of this system lies in its complexity, as it becomes less viable to have three drones running simultaneously, knowing that the reconnaissance drone system could easily be incorporated into one of the direct combat drones.

Another example of a firefighting drone is Zhun [9]. This example was developed by Walkera Technology Co. Ltd. and was designed to combat urban fires, more specifically

fires in very high buildings. Through Figure 10, it is possible to get a sense of how this drone works when it is fighting a fire.

Figure 10 - Drone Zhun operating (extracted from [9]**)**

This drone is equipped with a battery that allows the drone to have 35 minutes of flight autonomy. Besides, it has a pressurized water reservoir and also a fire extinguishing bomb with a night vision targeting system.

The limitation of this system comes from the fact of having a built-in reservoir, which cannot be too large and heavy thus limiting suppression capacity. In this way, the drone becomes more suitable for small fires.

In Latvia, a very interesting solution for firefighting drones was also developed, which is shown in Figure 11. This drone was designed by Aerones [10] to help combat urban fires, especially in high-rise buildings. As is seen in Figure 12, this drone can go up until 300 meters high, which is considerably higher than what can be achieved with fire escape ladders.

Figure 11 - Aerones' drone operating (extracted from [10]**)**

To reach the height of Aerones' drone, this drone needs the support of 28 motors that are powered by batteries with autonomy for 30 minutes. The drone takes approximately 6 minutes to reach 300m high, which represents 20% of the battery's autonomy time. Thus, to make it feasible to use this drone, in addition to the batteries, the drone is connected by

electrical cables that supply power from the ground to the drone. The water supply for the drone is made by a tank that is on the ground and is connected to the drone through a hose. In this way, the inconvenience of the drone from Walkera Technology Co. Ltd. is solved, with no limitation on the amount of water available.

Figure 12 - Illustration of the advantage of Aerones' drone (extracted from [10]**)**

2.2. Hotspot detection using IR sensors

One of the main focuses of this thesis is the identification of hotspots through an IR sensor. The article "Early Forest Fire Detection Using Drones and Artificial Intelligence" [11] introduces a patrolling platform, comprised of two UAVs whose purpose is to detect hotspots. For this purpose, the platform is equipped with thermal and optical cameras that capture videos and images continuously. These videos and images are sent to a base station to assist firefighters in decision-making. The platform in question includes two UAVs. One of the UAVs acts at a high altitude and makes long-term observations following a certain route. If a hotspot is detected, this UAV activates an alarm and sends its GPS coordinates to the base station. However, this UAV may not make correct measurements due to its high altitude. Thus, to reduce the number of false alarms, a second UAV is used, which has the function of confirming the existence of the hotspot detected by the first UAV. This second UAV will fly to the GPS coordinates given by the first UAV and make a more detailed

observation of the location. If the hotspot is confirmed, the second alarm for the base station will be triggered. Figure 13 represents a schematic of this description.
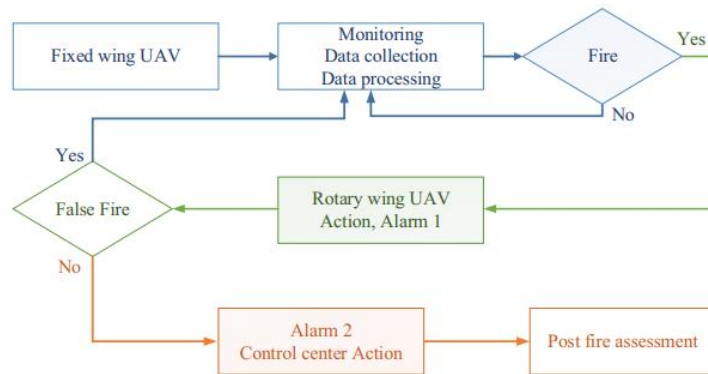
Figure 13 - Flowchart of system operation (extracted from [11])

The drones used in this work are of two distinct types: fixed-wing UAV and rotary-wing UAV. The first, which is represented in Figure 14 a), can fly higher and faster, in addition to having greater autonomy. On the other hand, the second drone, which is represented in Figure 14 b), is more agile, being able to lift and land vertically. The communication between the drones and the base station is done through two channels. One is used for data transfer and control, while the other is used for real-time video transmission.

a)   b)

Figure 14 – a) Fixed-wing UAV (extracted from [11]); b) Rotary-wing UAV (extracted from [11])

The drone that flies at medium altitude is equipped with a thermal camera with great zoom capacity and that works with a resolution of 640x480. The thermal camera of the low altitude drone is characterized by having a high resolution and by resisting adverse conditions such as rainy and foggy environments.

Finally, coupled to this platform is a system that uses artificial intelligence to recognize flames. For this, it is necessary to communicate between the drone's cameras and an on-board computer, responsible for image processing.

The article "Low-Cost System for Early Detection and Deployment of Countermeasures Against Wild Fires" [12] relates a low-cost solution of a modular system of the Master-Slave type to detect hotspots and create orders to target jets of water on those hotspots, from a water sprinkler. The architecture of this project is represented in Figure 15, where S represents the slave node, WS represents the water sprinkler and P represents the pressure sensor. Slaves nodes are responsible for reading and pre-processing data from the built-in flame sensor. These data consist of the temperatures read and are sent to the Master node. The Master node is connected to the Internet and aims to monitor the data collected and generate alarms. The alarm will be activated if a hotspot is detected, and the water sprinkler system will be activated immediately. Pressure sensors are used to ensure that there is sufficient pressure in the water sprinklers.
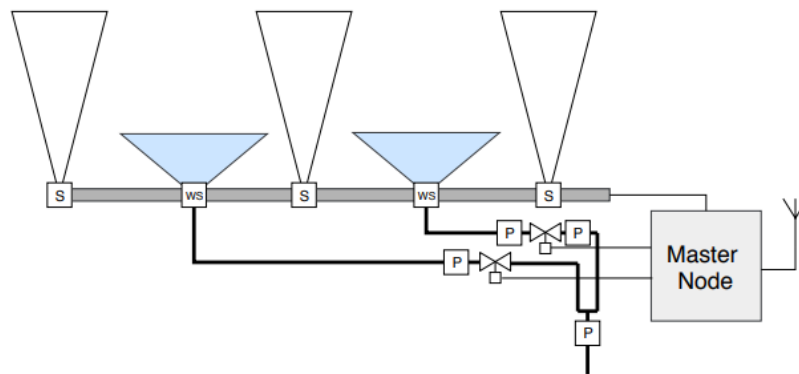
Figure 15 - Master-Slave system illustration (extracted from [12])

In this project, the detection of the hotspot is made from digital non-contact thermometers. This is because the objective is to build a low-cost system and the cost of a thermal camera (for example, a Lepton 3.5) is relatively high. However, these digital thermometers have the drawback of outputting the average temperature of each frame. If the thermometer is very close to the flame, the average temperature will be high because the flame occupies a large part of the frame. If the thermometer is far away, the frame will cover a larger area and the flame temperature will not have much influence when calculating the average temperature. This is confirmed by the experimental results of the article in question, which state that for short distances these thermometers read almost immediately and effectively the hotspots.

The article "Autonomous System for Wildfire and Forest Fire Early Detection and Control" [13] proposes an autonomous firefighting system that is at ground level and which

is represented in Figure 16. When the system detects a hotspot through an IR camera, an alarm is triggered, and a waterjet is directed to extinguish or delay the progress of the fire.
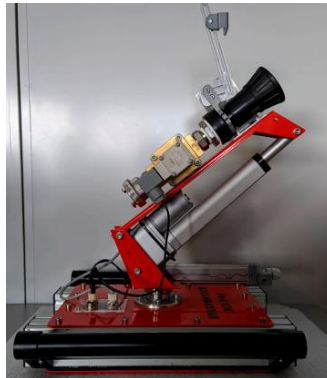
Figure 16 - Example of firefighting system used (extracted from [13])

The pumping of water is done through a nozzle that is built into a platform that rotates along different axes (pan and tilt). The flow of water is regulated using a solenoid valve. The image is captured using a low-cost, low-resolution IR sensor that is connected to a microcontroller. This microcontroller uses a wireless network to establish contact with the system user. The other purpose of the microcontroller, in addition to allowing remote control, is to control the pan and tilt platform and the solenoid valve. Through Figure 17 it is possible to observe schematically how the system works.
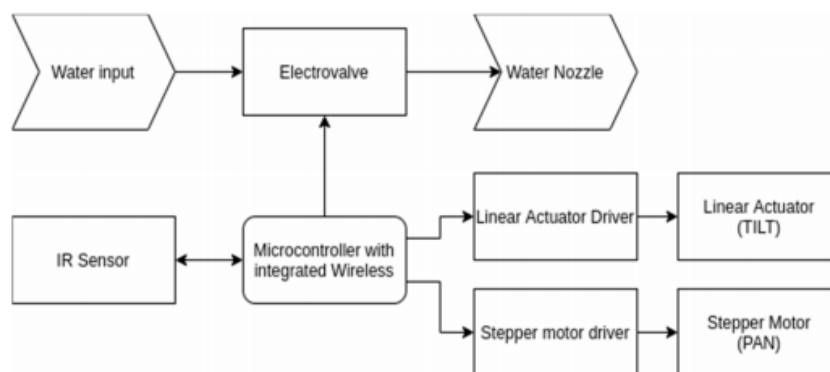
Figure 17 - Flowchart of system operation (extracted from [9])

This article introduces a basic approach to the analysis of the trajectory of the waterjet, which is also very important for the development of the project of this thesis. In this article, a parabolic trajectory was considered, and it was assumed that the waterjet acts as a stream of water spheres with a radius of 0.025m, launched at 40m/s. A drag coefficient of 0.5 was also assumed and there would be no dispersion of the waterjet caused by the wind. Another consideration taken was that the flight time of each water sphere is approximately 1s.

3. WORK DEVELOPMENT

3.1. Matrix features

Lepton 3.5 is a radiometric capable IR camera that captures images in the infrared spectral band (wavelength between 780nm and 1mm) with a resolution of 160x120 pixels. The radiometric characteristic of the sensor means that it was calibrated to estimate the surface temperatures in the captured images from their IR emission. By combining this data with the data from the Optical Flow sensor, it is possible to determine with great precision the location of the hotspot. In the array layout, the 160 pixels are distributed horizontally, and the 120 pixels are distributed vertically. Lepton 3.5 technical features can be consulted in [14].

3.1.1. Vertical features

Relatively the vertical characteristics in the matrix, it is necessary to consider not only the number of pixels but also the vertical angle of view. According to the Lepton 3.5 technical sheet, the vertical angle of the camera is 57°.

Knowing the vertical angle of the camera and the number of pixels along the vertical axis of the matrix, we are able to calculate the vertical unit angle. This angle represents the angle given by each pixel along the referred axis and is important when calculating the vertical coordinate of the hotspot. It is a fixed value since it represents the product between two characteristics of the thermal camera and is calculated by equation 1.

$$\alpha_{unit.V} = \frac{\alpha_V}{n_{pix.V}} = \frac{57}{120} = 0.475 \tag{1}$$

The 45° installation angle of the Lepton 3.5, together with the 57° vertical opening angle will cause a blind angle (α'$_{blind}$). This angle is between the bottom of the matrix and a vertical line that goes from the drone to the ground. Figure 18 shows the blind angle, and its value is α'$_{blind}$=16.5° considering a drone tilt angle of 0° (drone levelled). The tilt angle measures the drone's inclination, which occurs due to the action of the wind or the drone's movement. Equation 2 shows the blind angle.

$$\alpha_{blind} = 16.5 + \alpha_{tilt} \tag{2}$$
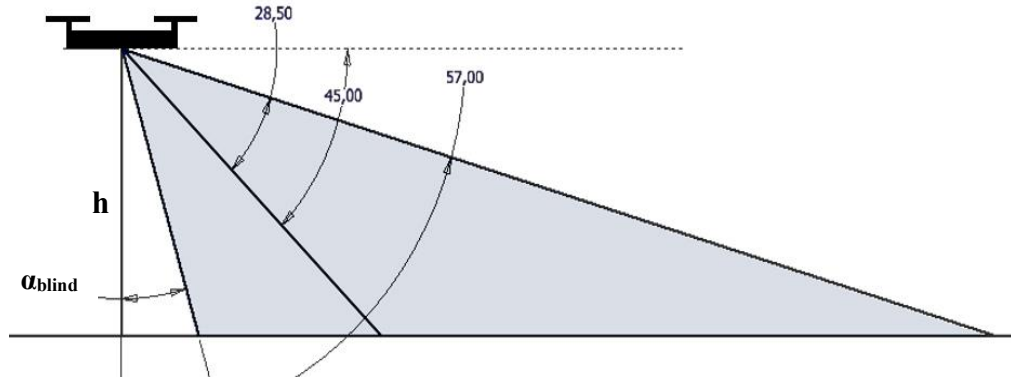
Figure 18 - Vertical angles representation, considering a tilt angle of 0º (drone perfectly horizontal)

3.1.2. Horizontal features

The horizontal characteristics of the matrix are also dependent on the horizontal angle of view and the number of pixels in that direction. According to the Lepton 3.5 technical sheet, it is known that the horizontal angle of view (α_H) is 71º, comprised of over 160 pixels. For this direction, it is necessary to calculate the horizontal unit angle. This angle is calculated by equation 3.

$$\alpha_{unit.H} = \frac{\alpha_H}{n_{pix.H}} = \frac{71}{160} = 0.444 \tag{3}$$

To determine the length of the array, the horizontal distance between the drone and the bottom of the array is required. This distance is called blind distance and depends on the value of the blind angle and the altitude at which the drone is. To calculate this distance, equation 4 is used.

$$d_{blind} = h.\tan(\alpha_{blind}) \tag{4}$$

Figure 19 makes it easier to visualize the measures involved in calculating the matrix length. This length increases as the coordinate i increases because the inclination of the IR sensor turns the matrix into a trapeze. Thus, the length of the matrix is given by equation 5.

$$L_i = 2.\left[(d_{blind} + i.\alpha_{unit.V}).\tan\left(\frac{\alpha_H}{2}\right)\right] \tag{5}$$
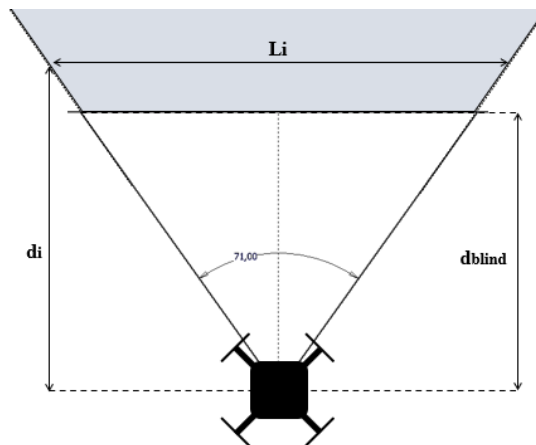
Figure 19 - Drone top view representation

3.2. Hotspot distance determination

Through the output given by Lepton 3.5, it is possible to determine where the hotspot is located. To do this, it is necessary to check the intensity of value assigned to each pixel in the matrix and see which pixel has the highest value, meaning the highest temperature. To guarantee that the hotspot detected is fire, the pixel value must be higher than 100ºC. More important than knowing the value associated with that pixel, is knowing its position in the matrix, corresponding to i line and j column coordinates. Through these coordinates, it is possible to calculate how far the drone is from the hotspot and the drone distance to the ground. In this work, will be assumed that the ground is flat. The coordinates of the hotspot will have the nomenclature (i_{Tmax}; j_{Tmax}).

By combining the characteristics of the matrix (listed in subchapter 3.1) with the obtained coordinates it is possible to determine the distance the hotspot is found by equations 6 and 7. This hotspot is also illustrated in Figure 20.

$$x_{Tmax} = h.tan[(120 - i_{Tmax}).\alpha_{unit.V} + \alpha_{blind}] \tag{6}$$

$$y_{Tmax} = x_{Tmax}.tan\,[\alpha_{unit.H}.(80 - j_{Tmax})] \tag{7}$$

Figure 20 - Representation of a detected hotspot

3.3. Waterjet trajectory

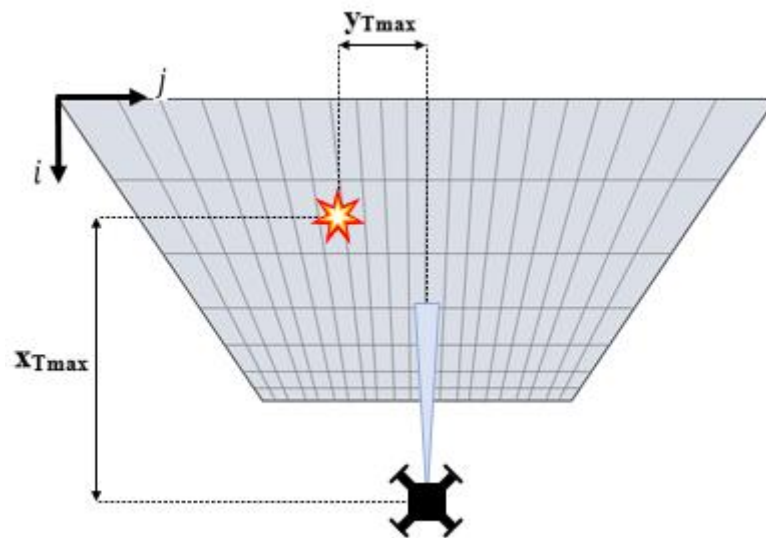The trajectory defined by the waterjet from the nozzle to the ground depends on the waterjet velocity on the nozzle, the nozzle geometry, water pressure, nozzle location and angle, and exterior disturbances. To determine water exit velocity, it will be necessary to use an experimental approach. The approach consists, firstly, of counting the time needed to fill a container with a predetermined volume. In this way, it is possible to calculate the volume flow. An important requirement for this step is that the volume flow must be constant. The second step is to measure the nozzle diameter and determine its area. Then it is possible to calculate the waterjet velocity on the nozzle.

3.3.1. Aerodynamic parameters

Aerodynamic parameters must be considered when studying cases in a real context. If these parameters are disregarded, the results obtained will not correspond to the situation closest to reality and may present quite significant deviations. For this case, the airflow effects on the waterjet will be studied, being the contact area between the waterjet and the airflow, the aerodynamic resistance coefficient, the airflow velocity, and direction, and also the air density.

Relating these parameters, it is possible to obtain the force that the airflow exerts on the waterjet. For this, the approach of [15] and [16] allows to find out the equation 8, which

shows the force applied on a waterjet and it is important to determine the waterjet acceleration.

$$F_D = \frac{\rho.A.C_D.v^2}{2} \tag{8}$$

3.3.1.1. Effect of incident air flow in the waterjet

The effect of incident airflow in the waterjet is very difficult to convert to analytical terms. Thus, it will be considered that the waterjet consists of a set of droplets, as described in [17]. In this article, a sprinkler was used to project water droplets. The conditions used to study the behaviour of the droplets were the wind speed, the downwind direction, and the zero-wind condition. Also, it was considered a constant pressure for all wind conditions (300kPa). To determine the drag coefficient, it is necessary to analyse some parameters such as the average diameter of the waterjet droplets and also the shape of these droplets.
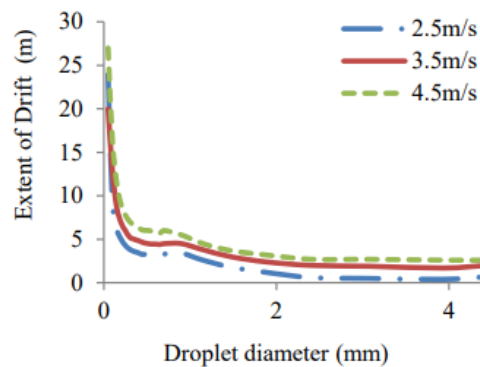
Figure 21 - Waterjet drift compared with droplet diameter (extracted from [17]**)**

Figure 21 was taken from [17] and relates the drift that occurred in the waterjet with the diameter of the droplet, for three different airflow speeds. What is observable is that, for the three wind speeds, the larger the diameter of the droplet, the smaller the drift. It is also possible to observe in the three cases that the drift stabilizes for droplet diameters greater than approximately 0.002m.

There is another article [18] that relates the longitudinal drift behaviour of droplets, using a more experimental approach, compared with [17]. To evaluate the longitudinal drift behaviour of droplets, tests were made in a wind tunnel. This wind tunnel had accoupled a wind generation system, followed by a spraying system, that in its turn is followed by a spray droplet collector. This assemble is represented in Figure 22.
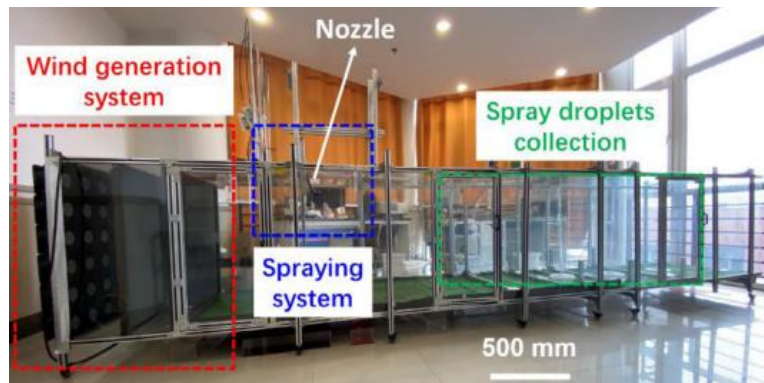
Figure 22 - Assemble of wind tunnel (extracted from [18]**)**

Some of the results obtained in this wind tunnel are represented in Figure 23. According to this figure, the smaller is the droplet, the biggest is the longitudinal drift. That conclusion is in line with the conclusion taken by [17].
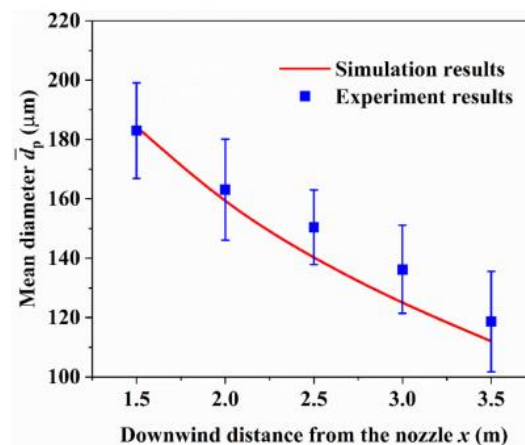
Figure 23 - Comparison between experimental results and simulated results (extracted from [18]**)**

To determine some of the factors, it is necessary to know not only the nozzle diameter (Dnozzle) used in this work but also the water outlet pressure in the nozzle (Pnozzle). For this work, Dnozzle = 0.0023m and Pnozzle = 101.325kPa were considered. Through these two values, it is possible to calculate the R factor. This factor is given by the equation 9 and is important for determining the average diameter of the droplet (d_{50}). The average diameter of the droplet is represented in the equation 10.

$$R = \frac{D_{nozzle}}{P_{nozzle}} = \frac{0.0023}{101325} = 0.0000000227 \; m/Pa \tag{9}$$

$$d_{50} = 0.31 + 11900 \cdot R = 0.31 + 11900 * 0.0000227 = 0.58 mm \tag{10}$$

Another aspect considered by the authors of the article is the percentage of droplets with a diameter smaller than d (Pv).

$$Pv = 100 \left[1 - e^{-0.693 . \left[\frac{d}{d_{50}} \right]^n} \right] \tag{11}$$

This percentage is defined by the equation 11 and its behaviour is represented in the Figure 24. The graph represents the Pv variation for a nozzle pressure of 101.325 kPa and 200kPa. What can be observed is that the increase in the pressure in the nozzle favours the increase in the percentage of smaller droplets, which makes the drift of the waterjet greater.
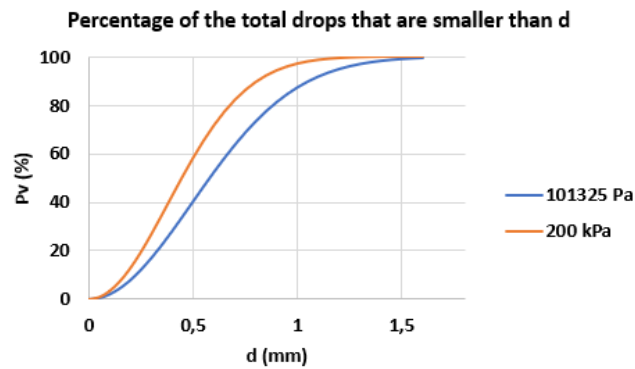
Figure 24 - Behaviour of percentage of drops smaller than d, for different pressures

The use of the average diameter of the water droplets is fundamental for the calculation of the Reynolds number. This value characterizes the flow of water and is also used to determine the drag coefficient. To determine this coefficient, the equation 12 is used.

$$C_D = \left[\left(\frac{24}{Re} \right)^{0.52} + 0.32^{0.52} \right]^{\frac{1}{0.52}} \tag{12}$$

However, to know the drag coefficient, it is necessary to know the flow speed first. To obtain this speed, the volume flow is related to the transversal area in the nozzle, as seen in the equation 13.

$$v = \frac{Q}{A_{section}} \tag{13}$$

To determine the volume flow (Q), an experimental test was made, which consisted of filling a container with water for a stipulated period. After that, the container was weighted. With this data, it was possible to determine the volume flow using the equation 14. This test took 1 minute (t), so the mass of water (m_{water}) obtained was 1.236kg.

$$Q = \frac{\frac{m_{water}}{\rho_{water}}}{t} = \frac{\frac{1.236}{997}}{60} = 0.0000207 \ m^3/s \qquad (14)$$

Where:

m_{water} - mass of water (kg)

ρ_{water} – water density (kg/m^3)

t - experiment time (s)

Knowing the volume flow, it is possible to use the equation 15 to determine the flow velocity.

$$v = \frac{Q}{A_{section}} = \frac{0.0000207}{\frac{\pi*0.0023^2}{4}} = 4.97 \ m/s \qquad (15)$$

Finally, with the value of the kinematic viscosity of the air, which is $\vartheta=1,85\mathrm{x}10^{-5}$ m^2/s, we can calculate the drag coefficient.

$$C_D = \left[\left(\frac{24}{Re}\right)^{0.52} + 0{,}32^{0.52}\right]^{\frac{1}{0.52}} = \left[\left(\frac{24}{\frac{v.d_{50}}{\vartheta}}\right)^{0.52} + 0.32^{0.52}\right]^{\frac{1}{0.52}} = 0.56$$

3.3.1.2. Area

As with the drag coefficient, the resistant area of the waterjet is also required. [16] relates the effects that the wind has on rain, through simulations made with sprayers. The same approach adopted by the authors to calculate the acceleration to which the raindrops are subjected was used in this work. In [16], the authors related Newton's 2nd Law with the drag force suffered by the drops, as can be seen in the equation 16.

$$m.a_x = -\frac{\rho_{air}.V_R{}^2.A.C_D.e_x}{2} \qquad (16)$$

Where:

m - mass of a drop of water in flight (kg)

a_x - acceleration of the waterjet, according to X (m/s^2)

ρ_{water}- air density (kg/m^3)

V_R - relative velocity of the drop of water, in relation to the wind (m/s)

A - resistant area (m^2)

C_D - drag coefficient

e_x - X-component of the unit vector that gives the direction of V_R

The purpose of using this approach is simply to calculate the waterjet droplet resistant area. However, some parameters need to be calculated *a priori*, such as the accelerations suffered by the droplet of water, according to the X-axis (a_x), the relative velocity of the droplet of water, in relation to the wind (V_R), and also the X-component of the unit vector that defines the direction of V_R (e_x). Thus, these parameters are given by the equations 17, 18, and 19, respectively.

$$V_R = \sqrt{(u_x - w)^2 + u_y{}^2 + u_z{}^2}$$
(17)

Where:

u_i - waterjet velocity component, along the *i*-axis (m/s)

w - wind velocity (m/s)

$$e_x = \frac{u_x - w}{V_R}$$
(18)

$$x = v_{0x}.t + \frac{1}{2}.a_x.t^2 \Leftrightarrow a_x = -\frac{2(x - v_{0x})}{t^2}$$
(19)

The equation 19 was obtained through the laws of cinematics. The parameters used for the acceleration calculations such as *x*, which represents the distance along the X-axis that the waterjet reaches, and v_{0x} which represents the X-component of the waterjet velocity in the nozzle, were determined using experimental tests carried out in a wind tunnel. These tests are described in more detail in the Section 4. Flight time (*t*) can also be determined using the equation 26. Finally, it remains only to determine the mass of a droplet of water that is in flight. According to [16], the mass of a droplet of water must be determined by the equation 20.

$$m = \frac{1}{6}\rho_{water}.\pi.D^3$$
(20)

where *D* represents the diameter of the droplet and was calculated when determining the drag coefficient.

The water droplet resistant area cannot be directly calculated. It is necessary to determine the diameter of the droplet first. For this, the equation 16 was reformulated, replacing the mass (m) with the equation 20 and the area (A) with the equation 21.

$$A = \frac{\pi.D^2}{4} \tag{21}$$

In this way, the equation 22 was obtained, in which the diameter is a function of the acceleration suffered by the waterjet.

$$D = -\frac{4.\rho_{air}.C_D.V_R{}^2 e_x}{3.\rho_{water}.a_x} \tag{22}$$

The drag coefficient was calculated in the subsection 3.2.1.1 using the approach proposed in [17], and the accelerations suffered by the waterjet were determined based on the experimental tests described in section 4. After getting all accelerations, it was possible to calculate the correspondent droplet diameter. The mean value of droplet diameter was considered, and the value obtained was 0.571mm. Thus, the resistant area of water droplet can be calculated, through equation 18.

$$A = \frac{\pi.D^2}{4} = \frac{\pi * 0.571^2}{4} \Leftrightarrow A = 0.257 \; mm^2$$

3.3.1.3. Air density

For this case, it makes sense to analyse the variation in air density as the altitude of the drone increases. This relationship is given by equation 23, and it was found in [19]. The equation and involves several constants, which are:

- Air molar mass – M = 0.0289644 kg/mol

- Ideal gas constant – R = 8.31447 J/(mol·K)

- Adiabatic gradient rate – L = 0.0065 K/m

- Gravity acceleration – g = -9.81m/s^2

- Atmospheric pressure at sea level – p_0 = 101325 Pa

- Atmospheric temperature at sea level – T_0 = 288.15 K

$$\rho = \frac{M.\left[p_0\left(1-\frac{L.h}{T_0}\right)\right]^{\frac{g.M}{R.L}}}{R.(T_0-L.h)} \tag{23}$$

This drone must perform its functions up to a maximum height of 50m. In this way, it makes sense to calculate the density of the air close to the ground as well as the density at 50m in height. The objective is to know the difference in densities and see if it is possible to consider the constant air density, assuming a minimum error. The calculations are shown in Table 1.

Table 1 - Results of air density values for different altitudes

	$\rho_{calculated}$ (kg/m³)	$\rho_{predefined}$ (kg/m³)	Error (%)
h=0m	1.225	1.222	0.245
h=50m	1.219		

The error shown in Table 1 is given as a percentage and is neglectable. Thus, a constant value for air density will be considered as altitude increases. This value is $\rho=1.222$kg/m³.

3.3.2. Final waterjet trajectory

To find out the final trajectory of the individual droplet is necessary to resort the laws of kinematics. Through these laws, it is possible to know the position of the droplet at each moment. For this context, it is only necessary to know the time that the waterjet takes to reach the ground and it is also necessary to know the distance that the waterjet can reach. Figure 25 illustrates the distances that are important to know.
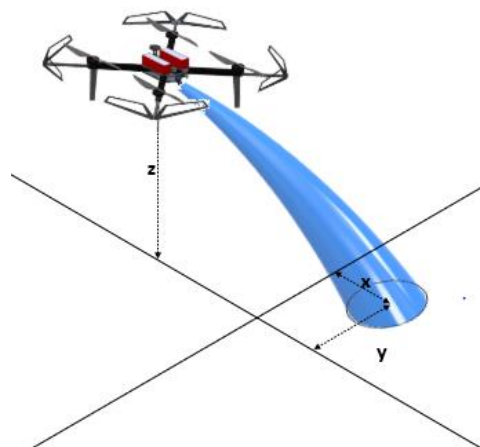
Figure 25 - Waterjet trajectory illustration

Equations 24 and 25 make it possible to calculate the distance on the X and Y-axis, respectively, that the waterjet can reach.

$$x = v_{0x}.t + \frac{1}{2}.a_x.t^2 \tag{24}$$

$$y = v_{0y}.t + \frac{1}{2}.a_y.t^2 \tag{25}$$

To find out how long the waterjet takes to reach the ground, equation 26 is used.

$$t = \frac{-v_{0z} - \sqrt{v_{0z}^2 - 2.(g-a_z).h}}{(g-a_z)} \tag{26}$$

In this equation, aerodynamic effects have to be considered, so it is necessary to replace a_z for equation 27.

$$a_z = -\frac{\rho_{air}.V_R^2.A.C_D}{2.m} \tag{27}$$

Where:

m - mass of a drop of water in flight (kg)

a_z - acceleration of the waterjet, according to Z-Axis (m/s^2)

ρ_{water}- air density (kg/m^3)

V_R – waterjet velocity, according to Z-Axis (m/s)

A - resistant area (m^2)

C_D - drag coefficient

3.4. UAV's movement

The distance travelled by the drone will not be equal to the vectorial sum of the distances determined when locating the hotspot. For a correct approach, importance must be given to the coordinates on which the waterjet will fall. To go towards the hotspot, the drone has to rotate around itself at a certain angle, and only after that, it must do a translation movement. The rotation angle (α_{UAV}) and the translation movement (d_{UAV}) are given by equations 28 and 29, respectively, and are illustrated in Figure 26.

$$\alpha_{UAV} = arctan\left(\frac{y_{Tmax}+y}{x_{Tmax}}\right) \tag{28}$$

$$d_{UAV} = \sqrt{(x - x_{Tmax})^2 + (y - y_{Tmax})^2} \tag{29}$$
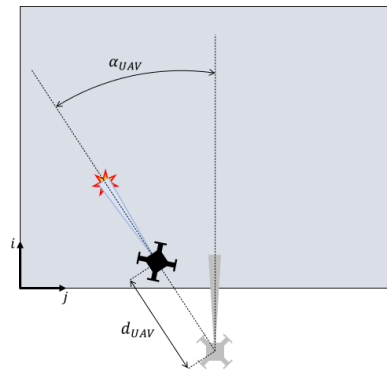
Figure 26 - Representation of the movements of UAV

3.5. Hardware communication

The correct communication between all sensors and boards is fundamental for the correct work of hotspot detection system. Figure 27 shows how all these components are connected, and it also shows which communication protocol is used in each connection. As is possible to observe in this figure, protocols like SI, I2C, UART and USB are used.

Figure 27 - Connections and communications protocols between components

3.5.1. Flight controller and optical flow

The connection between the flight controller Pixhawk 4 mini and the PX4Flow is made so that it is possible to measure in real-time the distance between the UAV and the ground. PX4Flow is connected to the flight controller via the I^2C port, as shown in Figure 28. For communication between both devices to occur, there must be a communication protocol. For this case, the protocol used is MAVLink. This pro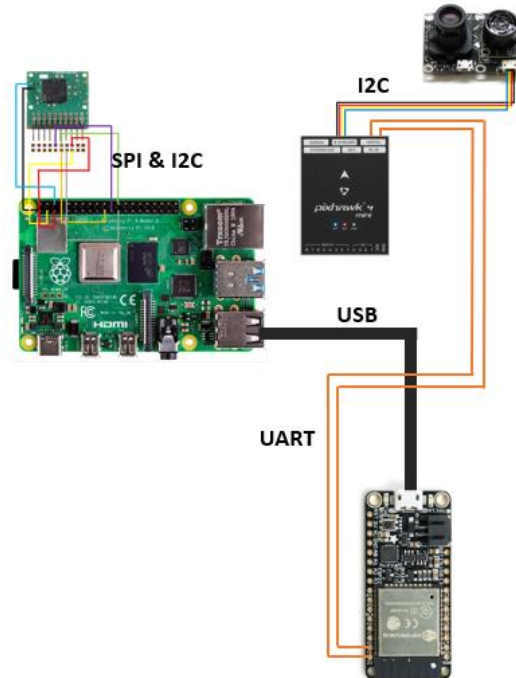tocol consists of a message with a specific structure that speeds up the reading of data from the sensor and that also allows messages to be sent to the sensor to control it. In [20] it is possible to find out some information about PX4Flow like its specifications, communications protocols, some manuals and libraries possible to be used to connect this sensor to flight controller.
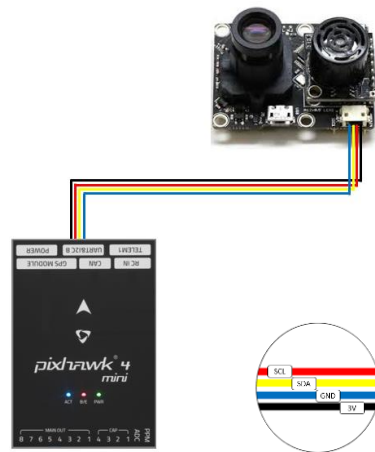
Figure 28 - Representation between flight controller and optical flow

3.5.2. Raspberry Pi and IR sensor

The IR sensor FLIR Lepton 3.5 is used to capture thermal images and detect hotspots. After detecting the hotspot, the sensor must send information that indicates where that same hotspot is. However, the connection between the IR sensor and Raspberry Pi 4 cannot be done directly. It is necessary to attach the Lepton Breakout Board to the IR sensor first, and the Raspberry Pi 4 must be connected to this board. The connection between the board and the Raspberry Pi 4 must be done as shown in Figure 29. In addition to the connections that are responsible for supplying the circuit (GND and 3V), it is necessary to connect the ports

that transmit data. To transmit data from the board to Raspberry Pi 4 there are two different protocols. One of them is SPI: this protocol uses pins like MOSI, MISO, SCK and CS. The other one is I2C: this one only uses SDA and SCL to transmit data. Figure 29 represents how the connection between Raspberry Pi 4 and Lepton Breakout Board V2.0 is made. This connection is based on an example showed in Flir Lepton website [21].
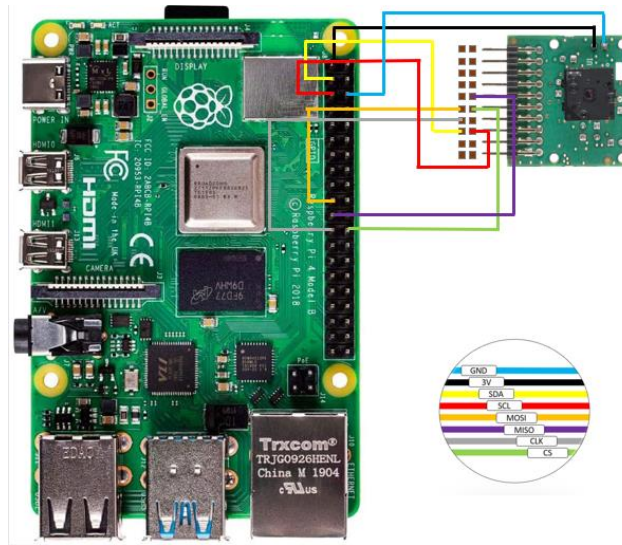
Figure 29 - Representation between Raspberry Pi 4 and Lepton Breakout Board V2.0

3.6. GUI implementation

In order to monitor the UAV in real-time, a Graphical User Interface (GUI) must be created. From the ground, the user should be able to send messages to the UAV to control its movement, and also should see the parameters given by the UAV. The communication between user and UAV only is possible due to a Wi-Fi connection, generated by Adafruit Huzzah32.
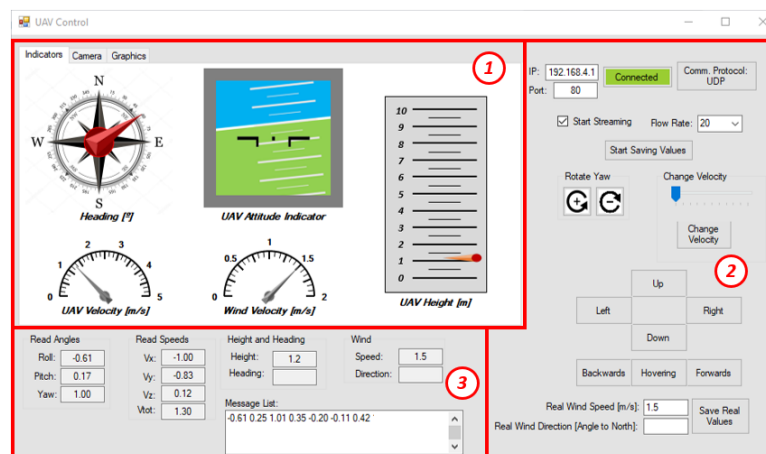
Figure 30 - Parts of GUI developed (Indicators page)

The GUI developed in this work is represented in Figures 30, 31, and 32, and it is divided into three different parts, with different functions. Part 1 is responsible to show by a graphical way the variation of UAV parameters. This part is also divided into other three pages, which are:

- Indicators: In this page, there are used some gauges to represent UAV parameters. These parameters are the UAV heading, attitude, velocity, and height. Also, there is another gauge that quantifies the wind velocity.

- Camera: This second page is responsible only to stream the thermal images caught by the IR sensor.

- Graphics: This page shows some graphics that allow the user to observe how the UAV parameters change while time passes. It is also possible to combine more than one parameter in the same graph, which is useful to compare different parameters. The parameters presented can be the Roll, Yaw, and Pitch angles, the UAV velocity, height, and heading, and the wind velocity.

Part 2 has not only some items related to the communication, but also has commands that are sent to the UAV and that can move it. The items responsible for communication consists of a button to connect and disconnect Wi-Fi, a button to change the protocol communication (is possible to use UDP and TCP), some text boxes that show the IP and Port, a checkbox that allows starting reading values, and a combo box that allows changing the rate that the values are received. The commands used in the interface can make the UAV rotate in its Yaw-Axis, can change the UAV velocity, and can translate the UAV to the right,

left, up, and down. It is also possible to make the UAV moves forward, backward, and make it hovers.

Part 3 has some text boxes that show UAV parameters like angles, velocities in different axis, heading, and height. It also shows the wind speed and direction. The message list presented in this part shows not only some UAV parameters but also the task that the UAV is doing at any moment.
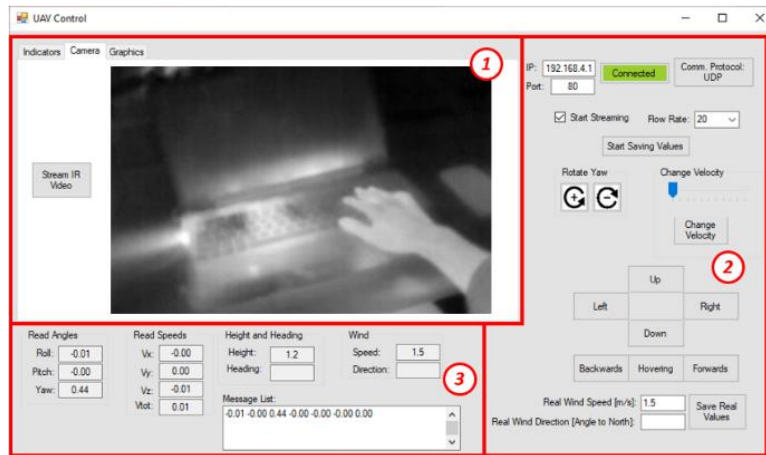

Figure 31 - Parts of GUI developed (Camera page)
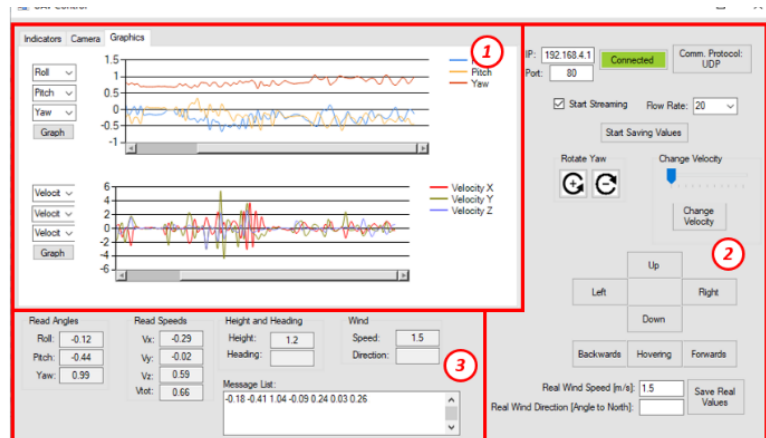
Figure 32 - Parts of GUI developed (Graphics page)

4. EXPERIMENTAL TESTS AND RESULTS

4.1. Aerodynamic parameters

During this project, it was necessary to make some experimental tests to determine some parameters that, analytically, would be difficult to determine. On the other hand, experimental tests are also important to validate the entire theoretical approach to the problem in question.

To determine the resistant area of the droplets that consist of the waterjet, the wind tunnel located at the Lousã aerodrome was used. These tests consisted of observing and analysing the behaviour of the waterjet when it is subjected to a controlled airflow.
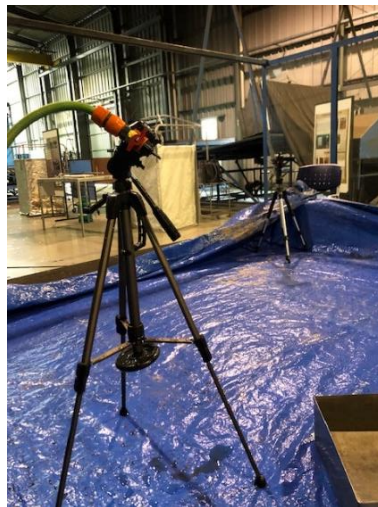
Figure 33 - Assembly of the nozzle

To perform these tests, a 0.0023m nozzle was used, which was attached to a hose through which the water was transported. The nozzle was placed 0.80m from the ground, attached to a tripod as shown in Figure 33. To measure airflow velocity more accurately, the hot wire anemometer, which is shown in Figure 34, was used. The anemometer was placed transversely to the airflow, and it was also attached to a tripod about 0.50m from the ground.
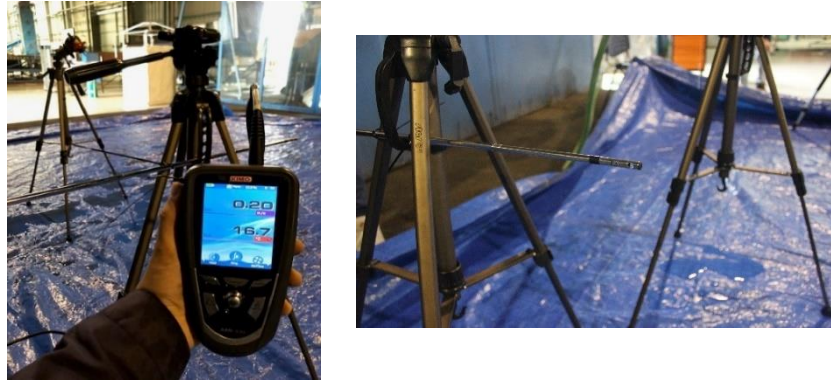
Figure 34 - Hot wire anemometer

In this work, it was considered that X-axis is aligned with waterjet direction, and Y-axis is perpendicular with waterjet direction, in the horizontal plan. The recording of waterjet trajectory was done through two cameras. One of the cameras was placed in front of the waterjet to observe the Y-axis deviations that could occur. The other camera was placed in profile with the waterjet, to observe X-axis deviations. Both cameras were installed at the same height as the nozzle, which was 0.80m from the ground. Figure 35 a) schematically represents the positioning of the cameras, the nozzle, and the hot wire anemometer. Figure 35 b) shows a photograph of this whole scheme assembled next to the wind tunnel.

a)   b)

Figure 35 - a) Representation of the entire assembly; b) Real image of the entire assembly

In carrying out these tests, three variables were considered: the inclination of the nozzle (γ), the speed of the airflow (U), and also the angle of incidence between the airflow and the waterjet (ϕ). Regarding the inclination of the nozzle (γ), tests were performed with

γ=0º with the horizontal as shown in Figure 36 a), and at γ=45º with the horizontal, as shown in Figure 36 b).

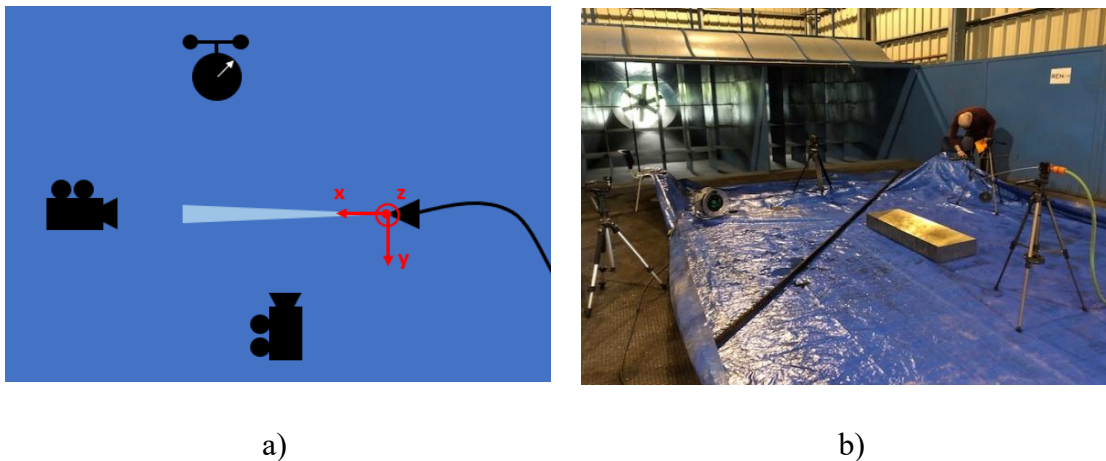a)   b)
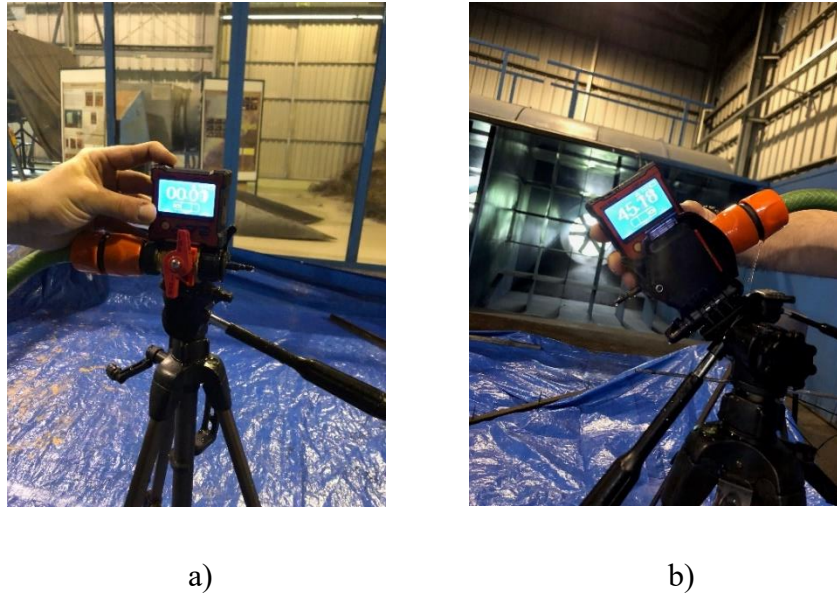
Figure 36 - a) Nozzle at 0º; b) Nozzle at 45º

For each angle of inclination of the nozzle, measurements were made without airflow and with different airflow velocities. First, measurements were made without airflow (U=0m/s), and then the flow velocity was increased at 0.5m/s intervals until 3.5m/s was reached. Finally, the last variable consisted of the angle of incidence between the airflow and the waterjet (ɸ). First, the waterjet was placed transversely to the direction of the airflow, that is, at ɸ=90º as seen in Figure 38 a). After carrying out the tests for the different slopes of the nozzle and different flow velocities, the entire assembly was rotated 45º, so that the waterjet hits 45º with the airflow (ɸ=45º). This assembly is represented in Figure 38 b). After all the tests were carried out in this position, the entire assembly was rotated again so that the waterjet was directed in the opposite direction to the airflow (ɸ=0º). This experimental setup is shown in Figure 38 c). Figure 37 schematically represents the experimental setups shown in Figure 38. This figure also shows in a more simplified way how the angle of incidence between airflow and waterjet (ɸ) varies.

a)   b)   c)
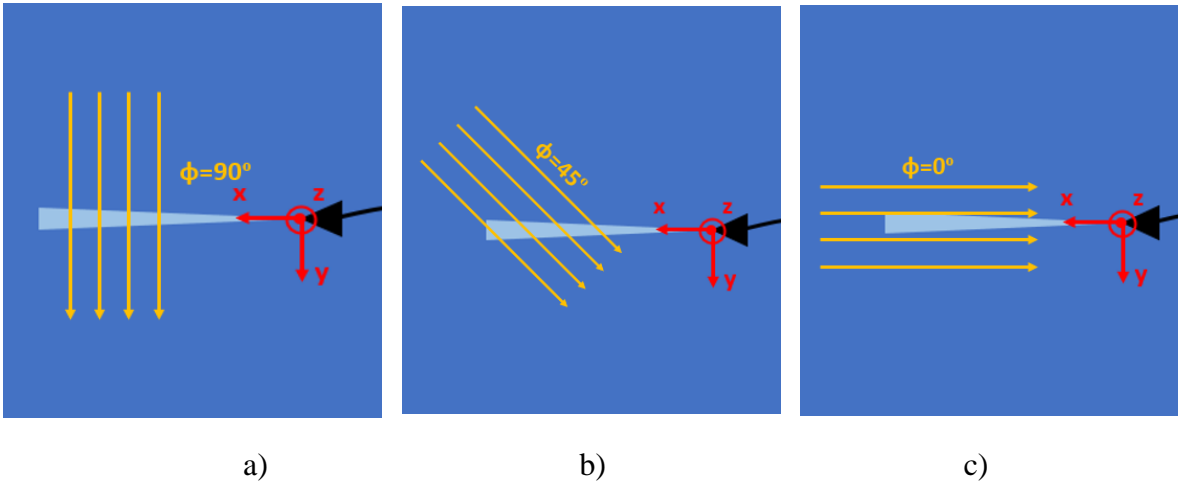
Figure 37 - Different angles of incidence between airflow and waterjet: a) φ=90º; b) φ=45º; c) φ=0º

a)   b)

c)
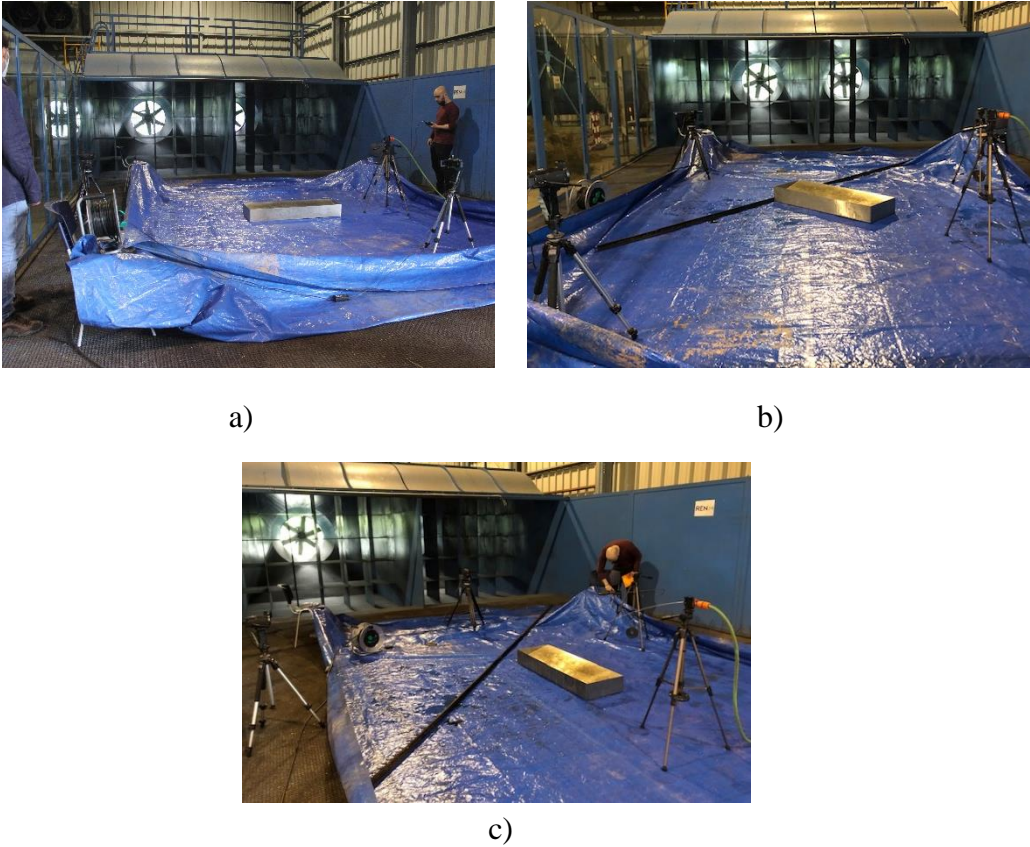
**Figure 38- a) Waterjet at 90º with airflow; b) Waterjet at 45º with airflow; c) Waterjet at 0º
with airflow**

The results obtained were captured by the two cameras used in the tests. Based on these videos, four frames were captured for each nozzle position (γ), each airflow speed (U), and each angle of incidence (ϕ). Then, the average values for the sets of four frames of each test were obtained and these average values were used. This procedure was repeated twice. A first time to analyse the results of the front camera, and a second time to analyse the results of the profile camera. Figure 39 shows the axis system used in these tests, so as it is noticeable, the front camera allows to analyse the drift according to the Y-axis and the profile camera allows to analyse the deviations according to the X-axis.
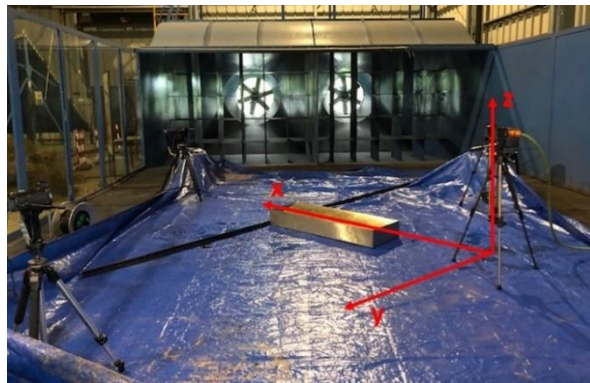
Figure 39 - Representation of the axis system

Also, Figure 40 a) and 40 b) show how the waterjet drift was measured according to Y-axis and X-axis, respectively. In these figures, the orange line represents the waterjet trajectory considering no airflow, and the red line represents the waterjet trajectory considering airflow with a determined velocity.
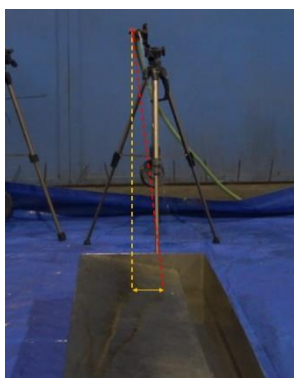
a)   b)

Figure 40 - a) Representation of the Y-drift; b) Representation of the X-drift

After analysing all the necessary measurements for all sets of variables, graphs were generated to facilitate the analysis of the waterjet drift. The Graph 1 a) shows the waterjet drift according to the X-axis for situations in which the nozzle angle was 0º. What is possible to observe is that there is a constant increase in the waterjet drift as the speed of the air flow increases. The same happens when the angle of inclination of the nozzle was 45º, as represented by the Graph 1 b).
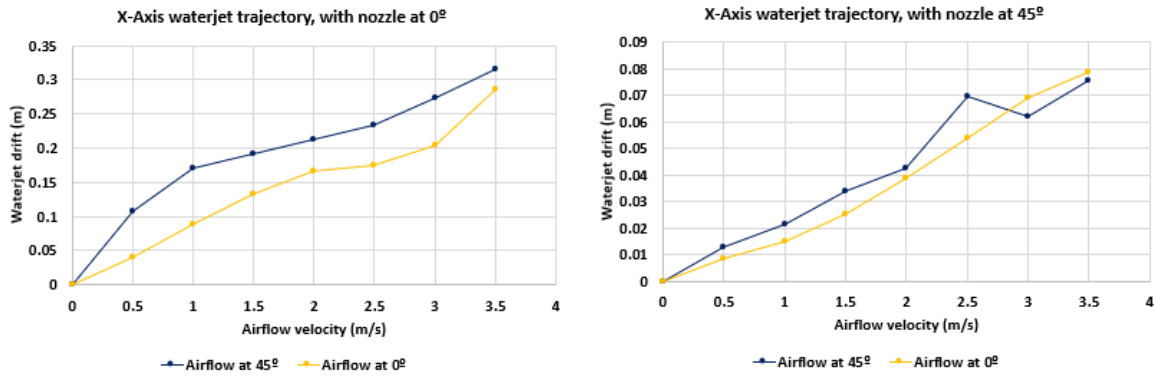
Graph 1 - X-drift with a) Nozzle at 0º; b) Nozzle at 45º

The Graph 2 compares the evolution of the waterjet drift along the X-axis when the airflow hits at 0º with the waterjet, for cases in which the nozzle is at 0º and 45º. To make it possible to compare these results, the percentage results of the waterjet drift were obtained, through equation 30, for the two situations in question. Through this graph it is possible to conclude that for both situations the evolution of the drift of the waterjet is constant and both results present very similar values. This allows to conclude that the behaviour of the waterjet for the different airflow velocities is independent of the angle of inclination of the nozzle.

$$\%_{Waterjet\ drift} = 100.\left[\frac{d_{v=0} - d_{v=i}}{d_{v=0}}\right] \tag{30}$$

Where:

$d_{v=0}$ – Distance targeted for waterjet, for airflow velocity equal to zero (m/s)

$d_{v=i}$ – Distance targeted for waterjet, for airflow velocity equal to i (m/s)

Percentual waterjet drift (X-Axis), with airflow at 0º
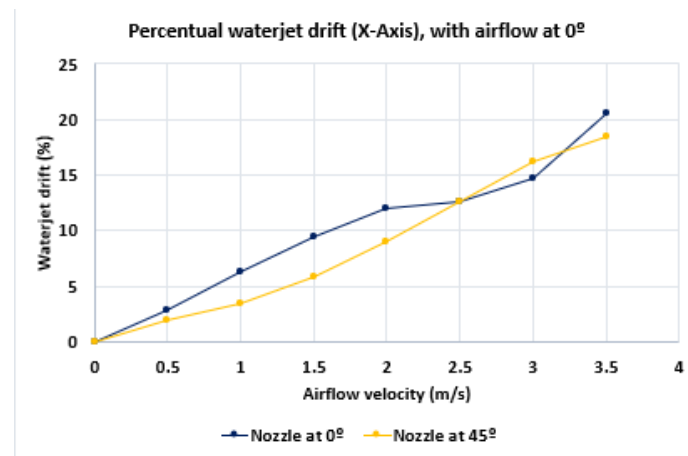
Graph 2 - Comparation between waterjet X-drifts

Analysing now the waterjet trajectory along the Y-axis, it is easily observed that the waterjet trajectory along this axis is very similar to the trajectory for the X-axis. Whether the nozzle is at 0º or when the nozzle is at 45º, there is always a near linear growth of the waterjet drift as the airflow speed increases. These behaviours can be seen in Graphs 3 a) and 3 b).
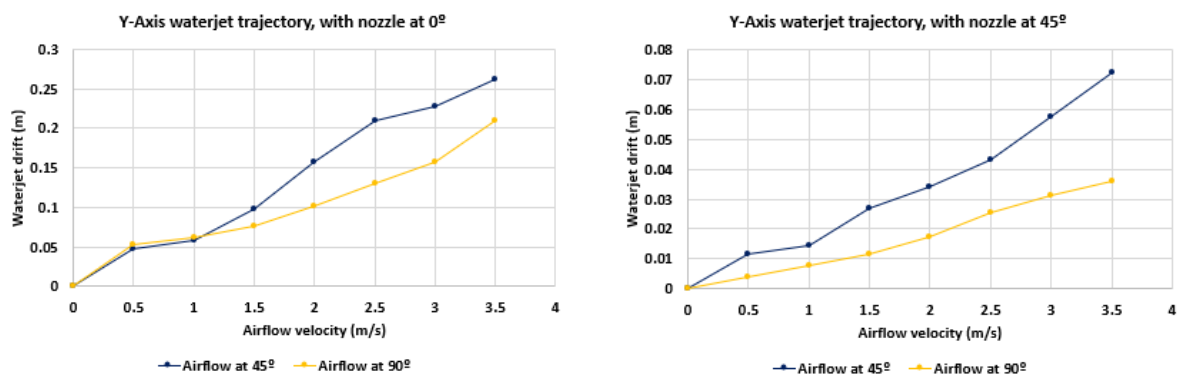
Graph 3 - Y-drift with a) Nozzle at 0º; b) Nozzle at 45º

However, the Graph 3 b) shows that the drift of the waterjet for a 45º flow incidence angle is substantially higher than the drift when the flow hits at 90º with the waterjet, which is not what would be expected. These results may be due to errors in the frame analysis procedure.

After getting all waterjet drifts, it was necessary to determine the correspondent acceleration that the waterjet was subjected. For each combination of variables, eight accelerations were determined, corresponding to the eight flow velocities used in the tests.

Thus, for a fixed drag coefficient, it was necessary to find the diameter of the droplet for each acceleration and find its average value. However, using an average value causes an associated error. If this error is not relevant, the average value of the diameter will be the value used for the remaining calculations.

For the calculation of the droplet diameter, only the results of the accelerations according to the X-axis were used. This was because the deviation along the Y-axis was more difficult to quantify through the frames captured from the videos and this can lead to significant errors. According to the X-axis, it is necessary to evaluate the results both for the airflow to hit at an angle of 0º and 45º, as well as for the inclination of the nozzle at 0º and 45º. The results obtained are shown in Table 2.

Table 2 - Experimental results for the droplet diameter

	X-Axis			
Nozzle tilt	**0º**		**45º**	
Airflow angle	**0º**	**45º**	**0º**	**45º**
Droplet diameter (mm)	1.787	2.264	0.764	0.799
	1.354	1.489	0.605	0.629
	0.993	1.059	0.468	0.486
	0.712	0.782	0.348	0.360
	0.498	0.556	0.244	0.253
	0.340	0.372	0.154	0.158
	0.209	0.225	0.075	0.078
	0.105	0.118	0.002	0.002
Average diameter (mm)	0.571			
RMSE	0.0935			

4.2.   Validation of hotspot detection algorithm

In order to validate the study made to the hotspot detection algorithm, it is important to do experimental tests. Despite the theme of this thesis consists not only in the detection of hotspots but also in the incidence of a waterjet on these hotspots, it was only possible to do experimental tests on the hotspot detection system. This happened due to several unforeseen events, which were unrelated to those who worked on this thesis (students and

supervisors). These unforeseen events are fundamentally component delays, caused by logistical issues related to Covid-19.

Figure 41 - Industrial crane holding drone during experimental tests

As can be seen in Figure 42, the entire hotspot detection system was incorporated into the drone chassis. This system consists of the Raspberry Pi 4, the Adafruit Huzzah 32 microcontroller, and the Lepton 3.5 IR sensor coupled to the Lepton Breakout Board V.2. After all this system was assembled, the drone was placed in an industrial crane that exists at the Industrial Aerodynamics Laboratory, in Coimbra, to simulate a flight situation, as the Figure 41 shows. For these tests, a hot air pistol was used to simulate the hotspot.
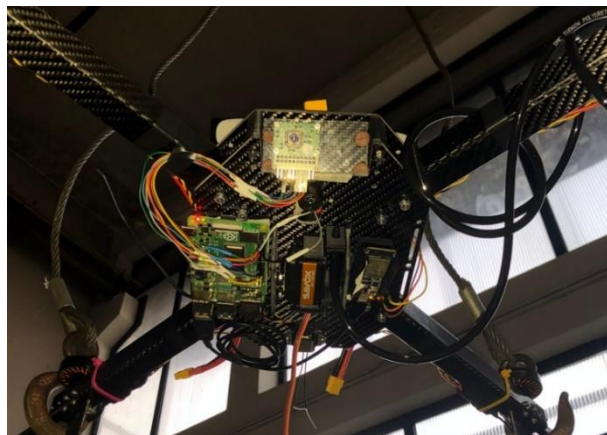
Figure 42 - Hotspot detection system incorporated in drone

In these experimental tests, three different hotspot locations were considered. For each location, IR sensor readings were taken considering four different altitudes of the drone. Figures 43 a), b) and c) show schematically the different hotspot locations. Figure 44 shows an example of the setup used in these experimental tests, where can be seen the drone hold by the industrial crane, and the hot air pistol simulating an hotspot. For the first test (Figure 43 a)) a distance of 1.10m on the X-axis and a distance of 0m on the Y-axis were considered. For the second test (Figure 43 b)) a distance of 1.10m on the X-axis and 0.74m were considered on the Y-axis. Finally, in the last test (Figure 43 c)) a distance of 1.65m on the X-axis and 0.74m on the Y-axis were considered. Both the measurements on the X and Y axes and the altitude of the drone were initially measured with a measuring tape so that it is possible to compare the real values with the values read by the sensors.
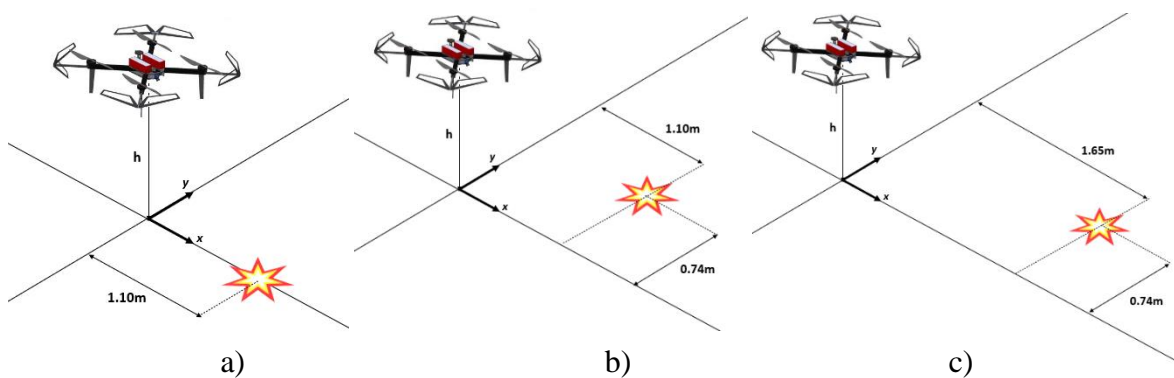

a)   b)   c)

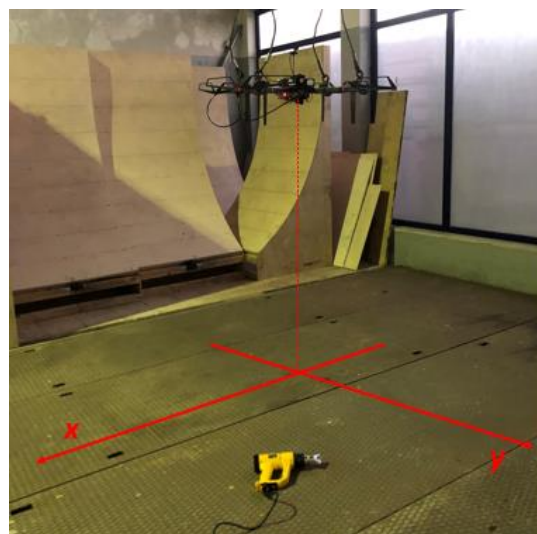**Figure 43 - Illustration of experimental tests: a) test 1; b) test 2; c) test 3**

Figure 44 – Set up of experimental tests

Table 3 - Comparison between the values read by the sensors and the real values for tests 1, 2 and 3

1					
Height (m)		X Distance (m)		Y Distance (m)	
Real	Calculated	Real	Calculated	Real	Calculated
1.07	0.98	1.1	1.24	0	0.08
1.47	1.33	1.1	1.16	0	0.12
1.74	1.57	1.1	1.06	0	0.07
2.04	1.81	1.1	1.04	0	0.08
RMSE		RMSE		RMSE	
0.0818		0.0429		0.0452	
2					
Height (m)		X Distance (m)		Y Distance (m)	
Real	Calculated	Real	Calculated	Real	Calculated
1.1	1.01	1.1	1.27	0.74	0.91
1.46	1.28	1.1	1.08	0.74	0.53
1.79	1.61	1.1	0.93	0.74	0.50
2.04	1.83	1.1	0.86	0.74	0.47
RMSE		RMSE		RMSE	
0.0856		0.0848		0.1133	
3					
Height (m)		X Distance (m)		Y Distance (m)	
Real	Calculated	Real	Calculated	Real	Calculated
1.1	1.02	1.65	2.13	0.74	1.18
1.39	1.21	1.65	1.92	0.74	0.78
1.9	1.72	1.65	1.68	0.74	0.79
2.17	1.93	1.65	1.35	0.74	0.59
RMSE		RMSE		RMSE	
0.0901		0.1551		0.1163	

Table 3 shows the results obtained through the sensors used, mainly the IR sensor and the sonar. These results are indicated in the "Calculated" columns. The values in the "Real" columns correspond to the values measured with the measuring tape. The results read by the sensors were monitored through a graphical interface (GUI), which is represented in Figure 45. As can be seen, this interface shows not only the drone's height values, but also the distances on the X and Y axes at which the hotspot is located. Also, in this interface it is possible to observe the thermal image generated by the IR sensor during the experimental tests. To evaluate the error between real values and measured values, Root Mean Square Error (RMSE) was used.

Through this table, it is possible to observe that the results measured by the sensors are not very different from the real results. Even so, the results that show the greatest discrepancy correspond to the results of the X-axis, for test 3. Tests 2 and 3 also show relatively high RMSE values.

The main causes of errors observed in the measurements of distances on the X and Y axes can have different natures. First, the error between the real height at which the drone is and the height measured by the sonar must be considered. This error occurs because the sonar is calibrated through a calibration line, and this calibration line has an associated error.

This is an important issue because the height of the drone is used to calculate the distances on the X and Y axes. On the other hand, it should be taken into account that during the experimental tests the drone was attached by steel cables to an industrial crane. In this way, the drone was always subject to slight rotations and balancing caused by these steel cables. These movements were enough for the drone to be misaligned with the defined axis system, which is represented in Figure 44
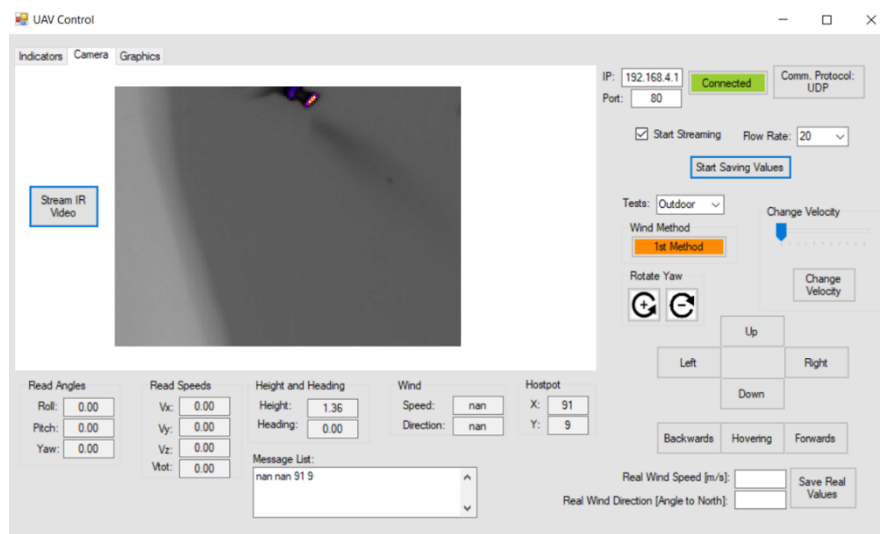
.

Figure 45 - GUI showing the hotspot and other parameters

5. CONCLUSION

This dissertation had as main objectives the detection of hotspots through an IR sensor coupled to a UAV and the development of an algorithm to determine the distance that hotspot was from the UAV. Furthermore, it was intended to study the effects of airflow on the waterjet that would hit the hotspot, and develop an algorithm to determine the movements that the UAV would have to make for the waterjet reaches accurately the hotspot.

For this, it was necessary to carry out a first research on studies by other authors who dealt with related issues. This research was very important, especially to better understand how these types of drones work and in which situations they can be applied. In addition, it was also important to analyse studies related to the behaviour of water droplets when they hit airflows. Studies related to the aerodynamic parameters of the waterjet were fundamental. Initially, the objective was to approach the waterjet as a single mass, and with the help of these studies, it was realized that the best approach would be to consider the waterjet as a set of water droplets. Thenceforth, the whole approach to aerodynamic parameters made a lot more sense.

A previous approach was also made to the sensors used in this hotspot detection system. This approach essentially served to know the characteristics of each sensor, especially the IR sensor, to develop an algorithm based on these characteristics. Furthermore, this analysis was important to find an efficient way of communication between all sensors. After knowing all these characteristics, it was necessary to proceed with the respective connection between the sensors and their programming. For this part of the thesis to be done successfully, the help of José Pedro Correia was essential. In addition, a Graphical User Interface (GUI) was also developed so that it was possible to monitor the drone remotely and observe its measurements in real time.

After all sensors communicated correctly, the experimental tests of this hotspot detection system were carried out. The results to be analysed from these experimental tests consisted of data read by the sensors, and data measured manually with a measuring tape. What is possible to observe is that the results between the data read by the sensors and the real data are similar, naturally having an associated error. This error was quantified through the RMSE, and what is possible to conclude is that this error increases both for the distance

on the X-axis and the Y-axis as the height of the drone increases. This error can have several causes, such as the balance of the drone during the tests, its off-centre, and bad manual measurements. In addition, the sonar has been calibrated with a calibration line, which also has an error associated with it. This calibration line may be a justification for the fact that the error increases as the drone's height increases.

During this thesis, some unforeseen events occurred, which were fundamental for not reaching the totality of the objectives of this thesis, mainly the realization of experimental tests with the drone flying autonomously. These unforeseen events consisted mainly of drone component delays due to the logistical anomalies that Covid-19 caused around the world. Even so, throughout the development of this thesis, it was necessary to acquire other components that were not planned to incorporate this hotspot detection system, but which became essential for this project to move forward. The main examples were the Raspberry Pi 4 and the Lepton Breakout Board V2. Despite all these adversities, the effort of the entire team, including students and supervisors, was essential for this thesis.

The research and development work for this thesis was quite challenging, because it treated on topics that are typically not so commonly addressed in a traditional Mechanical Engineering course: programming and sensors. However, throughout this thesis, it was possible to learn a lot about this area. The thesis theme is also quite interesting as it is a great example of how the evolution of science and technology can help in quotidian circumstances. Furthermore, using such equipment in firefighting reduces firefighters' exposure to fire, thus decreasing the probability of causing them traumatic injuries, or even death.

For future work, some improvements can be made. The conditions of experimental tests can be improved, especially about the way that the drone is suspended. Due to the unforeseen circumstances that have already been explained, it was only possible to carry out experimental tests on the hotspot detection system with the drone suspended in an industrial crane. Thus, it is proposed that in the future it will be possible to carry out these tests with the drone flying autonomously. There is other future work that is not an improvement, but a compliment. This work consists of carrying out experimental tests using not only the hotspot detection system but also the waterjet from the drone's nozzle.

6. BIBLIOGRAPHY

[1]   "Global Wildfire Information System (GWIS)," 2021. https://gwis.jrc.ec.europa.eu/apps/country.profile/continent/EU.

[2]   "Canadair CL-415 – Wikipédia." https://pt.wikipedia.org/wiki/Canadair_CL-415.

[3]   "GPIAAF." https://www.gpiaaf.gov.pt/.

[4]   PORDATA, INE, and DGS/MS, "PorData," *PorData*. 2019, [Online]. Available: https://www.pordata.pt/DB/Portugal/Ambiente+de+Consulta/Tabela.

[5]   Shark Robotics, "Colossus Robot," 2017. https://www.shark-robotics.com/shark-robots#rhyno.

[6]   J. Loureiro and G. Mogas, "DISPOSITIVO PARA COMBATE DE INCÊNDIOS POR PLATAFORMA SUSPENSA COM CONTROLO REMOTO," PT 109921 B, 2020.

[7]   G. Do LEE, "DRONE ANTI-INCENDIE POUR GRATTE- CIEL," 3 085 118, 2019.

[8]   C. J., "Forest fire extinguishment system using drone and method thereof," KR102209056B1, 2020.

[9]   "Zhun - Walkera," 2017. https://www.walkera.com/index.php/Goods/info/id/71.html.

[10] "Aerones Firefighting," 2018. https://www.businessinsider.com/aerones-firefighting-drones-2018-4.

[11] D. Kinaneva, G. Hristov, J. Raychev, and P. Zahariev, "Early Forest Fire Detection Using Drones and Artificial Intelligence," 2019, doi: 10.23919/MIPRO.2019.8756696.

[12] M. Antunes, L. M. Ferreira, C. Viegas, A. P. Coimbra, and A. T. De Almeida, "Low-Cost System for Early Detection and Deployment of Countermeasures Against Wild Fires," 2019, doi: 10.1109/WF-IoT.2019.8767331.

[13] L. M. Ferreira, A. P. Coimbra, and A. T. De Almeida, "Autonomous System forWildfire and Forest Fire Early Detection and Control," no. 6, 2020.

[14] "FLIR LEPTON® Engineering Datasheet," .

[15] J. Zhu, W. Li, D. Lin, and G. Zhao, "Study on Water Jet Trajectory Model of Fire Monitor Based on Simulation and Experiment," 2018, doi: 10.1007/s10694-018-

0804-1.

[16]   J. L. M. P. De Lima, P. J. J. F. Torfs, and V. P. Singh, "A mathematical model for evaluating the effect of wind on downward-spraying rainfall simulators," *Catena*, 2002, doi: 10.1016/S0341-8162(01)00171-0.

[17]   F. A. Dwomoh, Y. Shouqi, and L. Hong, "Analytical study of wind influence on in-flight sprinkler droplets," *J. Eng. Technol. Sci.*, 2015, doi: 10.5614/j.eng.technol.sci.2015.47.3.5.

[18]   S. Xue, X. Xi, Z. Lan, R. Wen, and X. Ma, "Longitudinal drift behaviors and spatial transport efficiency for spraying pesticide droplets," *Int. J. Heat Mass Transf.*, vol. 177, 2021, doi: 10.1016/j.ijheatmasstransfer.2021.121516.

[19]   "Density of air - Wikipedia." https://en.wikipedia.org/wiki/Density_of_air.

[20]   "PX4FLOW Smart Camera | PX4 User Guide." https://docs.px4.io/master/en/sensor/px4flow.html.

[21]   F. Lepton, "Getting started with the RaspberryPi and Breakout board V2.0," *Getting started with the RaspberryPi and Breakout board*. https://lepton.flir.com/getting-started/raspberry-pi-lepton/.